Probing hydrodynamic sound modes in magnon fluids using spin magnetometers

Joaquin F. Rodriguez-Nieva [1,*] Daniel Podolsky [2,3] and Eugene Demler[1,†]
[1]*Department of Physics, Harvard University, Cambridge, Massachusetts 02138, USA*
[2]*Department of Physics, Technion, Haifa 32000, Israel*
[3]*ITAMP, Harvard-Smithsonian Center for Astrophysics, Cambridge, Massachusetts 02138, USA*

(Received 10 January 2020; revised 15 August 2020; accepted 14 April 2022; published 12 May 2022)

The noninteracting magnon gas description in ferromagnets breaks down at finite magnon density where momentum-conserving collisions between magnons become important. Here we present a hydrodynamic description of spin systems with global SU(2) symmetry in the ferromagnetic phase. We identify a key signature of the collision-dominated hydrodynamic regime—a magnon sound mode—which governs dynamics at low frequencies. The magnon sound mode is an excitation of the longitudinal spin component with frequencies below the spin-wave continuum in gapped ferromagnets and can be detected with recently introduced spin qubit magnetometers. We also show that, in the presence of exchange interactions with SU(2) symmetry, the ferromagnet hosts an usual hydrodynamic regime that lacks Galilean symmetry. We show that our results are relevant to ferromagnetic insulators in a finite energy/temperature window such that dipolar and magnon–phonon interactions are negligible, as well as in recent experiments in cold atomic gases.

DOI: 10.1103/PhysRevB.105.174412

I. INTRODUCTION

The presence of symmetries and conservation laws can affect the universal dynamics of interacting quantum systems in dramatic ways. One example is the recently observed hydrodynamic regime in graphene where, in a wide range of temperatures, fast momentum-conserving collisions lead to viscous electron transport [1–6]. This unusual electron transport behavior, also proposed in a variety of other quantum systems [7–16], differs from the more conventional ballistic and diffusive regimes. The giant leap in our understanding of quantum transport that resulted from the study of hydrodynamics in graphene, combined with the advances in material synthesis and quantum metrology, motivates us to raise two new questions: (i) Are there other available experimental platforms to probe new hydrodynamic regimes in quantum materials? (ii) Can additional symmetries give rise to qualitatively distinct transport features?

We address these two questions by showing that (i) Heisenberg ferromagnets host an unusual hydrodynamic regime in a wide range of temperatures and frequencies when SU(2) symmetry is present, and (ii) we propose an experimental protocol to detect hydrodynamic modes using spin qubit magnetometers [17,18]. As we will see, the hydrodynamic regime is unusual because of the lack of Galilean symmetry, signaling the presence of a special reference frame in the system.

At low temperatures, the long-wavelength excitations in ferromagnets (magnons) propagate ballistically given the weak magnon–magnon interaction which renders relaxation processes inefficient. However, as temperature increases and the thermal magnon population occupies larger momentum states, *momentum-conserving* collisions give rise to a relaxation length ℓ which steeply decreases with temperature T and magnon density n [19]:

$$\ell = \frac{1}{na^{d-1}}\left(\frac{J}{T}\right)^{\frac{d+1}{2}}. \tag{1}$$

Here a is the lattice spacing, J is the exchange coupling, and $d \geqslant 2$ is the dimension (see Appendix A). For an intermediate temperature range such that Umklapp scattering can be neglected ($T \ll J$) but large enough such that $\ell \ll L$ for the characteristic length L of the system, hydrodynamic behavior emerges. For instance, for moderately small occupation numbers ($na^d \sim 0.1$) and temperature below the Curie temperature ($T/J \sim 0.2$), $\ell \sim 50\,\text{nm}$ is much smaller than a typical sample length $L \sim 10\,\mu\text{m}$ (here we used $a = 0.5\,\text{nm}$ and $d = 2$).

A key signature of momentum-conserving collisions is the existence of a gapless sound mode, even when the spin-wave continuum is gapped by a Zeeman field. As shown in Fig. 1, the sound mode is manifested as an excitation of the longitudinal spin correlator, $\langle \hat{S}^z \hat{S}^z \rangle$, where $\hat{S}^z$ is related to the magnon density n via $\langle \hat{S}^z \rangle = S(1 - na^2)$ and is analogous to a second sound in a superfluid [20–22]. As a result, spin fluctuation measurements can provide clear-cut signatures of the sound mode, as shown below. We distinguish magnon hydrodynamics from hydrodynamics in electron fluids where, rather than sound modes, the system hosts plasmon modes; this qualitatively distinct behavior arises because longitudinal charge fluctuations are mediated by long-ranged Coulomb interactions [23]. We also distinguish the sound mode from the previously studied "magnon BEC" [24–27] in which the physics is primarily governed by the dynamics of the ferromagnetic order parameter.

*Current address: Department of Physics, Stanford University, Stanford, California 94305, USA.
†Current address: Institute for Theoretical Physics, Wolfgang-Pauli-Str. 27, ETH Zurich, 8093 Zurich, Switzerland.

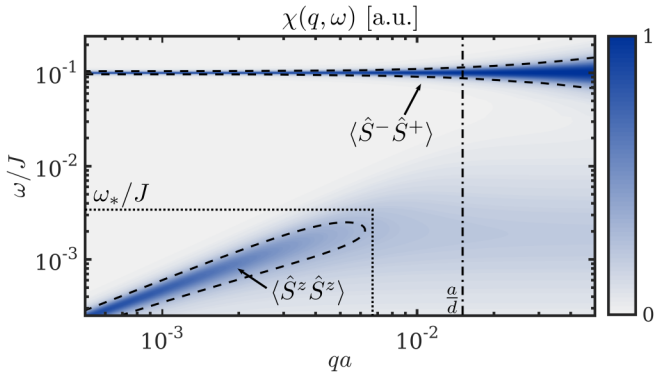

FIG. 1. Spectral function $\chi(q,\omega) = \chi_{+-}(q,\omega) + \chi_{-+}(q,\omega) + 4\chi_{zz}(q,\omega)$ exhibiting single magnon excitations at the Zeeman energy $\omega = \Delta$, induced by a finite $\langle S^- S^+ \rangle$, and a linearly dispersing sound mode at low frequencies induced by magnon density fluctuations, $\langle \hat{S}^z \hat{S}^z \rangle$. The sound mode is damped above frequencies ω_* by viscous forces.

One unique feature of magnon hydrodynamics is that the SU(2) symmetry constrains the collisions between quasiparticles, giving rise to a momentum-dependent magnon–magnon interaction which vanishes at $\boldsymbol{k} = 0$ [see Eq. (5)]. This feature bears important consequences. First, Galilean symmetry is *intrinsically* broken at all length scales and differs from usual hydrodynamics in lattice systems where Galilean symmetry is broken *only* at energy scales comparable to the single-particle bandwidth (i.e., when deviations from quadratic dispersion are sizable). While Galilean symmetry can also be broken in planar ferromagnets in the presence of spin textures [28–31], Galilean symmetry is broken with or without spin textures in isotropic ferromagnets. Second, vanishingly small scattering matrix elements suppress collisions between magnons and the magnon condensate that arises due to symmetry breaking. Such suppression justifies why the dispersion of magnons—the Goldstone modes of the ferromagnet—remain quadratic in the symmetry-broken phase, contrary to U(1)-symmetry breaking where interactions between quasiparticles and the condensate renormalize the quasiparticle dispersion and where a "two-fluid" description is necessary.

Previous works on hydrodynamics in ferromagnets assume momentum relaxation due to Umklapp scattering ($T \approx J$) or disorder, as first described by Halperin and Hohenberg [32]. Such momentum-relaxing effects give rise to diffusive particle and energy transport. Although a few authors [20–22] made the case for momentum-conserving hydrodynamic behavior in a magnon gas, there is little experimental evidence of this regime to date [33]. Arguably, the energy scales (∼meV) and wave vectors ($\gtrsim 1/a$) accessible by neutron scattering, the main probe of ferromagnets at the time, were too large to access the low-frequency, long-wavelength regime in which hydrodynamic sound modes live. In addition, the Hamiltonian of realistic materials has terms that break magnon number and momentum conservation, such as dipolar interactions and magnon–phonon interactions and, as a result, it is unclear whether such regime can exist in realistic materials.

We argue that recent experiments [34–39] have opened new pathways to observe and study hydrodynamic behavior in spin systems. First, ultraclean ferromagnetic materials, such as yttrium iron garnet (YIG), allow ballistic propagation of magnons in macroscopic scales without scattering by impurities and phonons. *Independent* control of temperature and chemical potential is possible via a combination of heating and driving and, therefore, enables us to explore all possible regimes from noninteracting magnon gases to interacting magnon fluids. In addition, magnetic spectroscopy with spin qubits allows us to access spin fluctuations at the energy and length scales relevant for hydrodynamics. Besides spin waves [34,35], such probes have been used to image single spins [40] and domain walls [41] and to study electron transport in metals [42]. Such probes could also be used to access the hydrodynamic regime in graphene [43] and 1D systems [44], to study magnon BECs in ferromagnets [45], and to diagnose ground states in frustrated magnets [46]. In addition, recent experiments in isolated cold atomic gases [36–39] now have access to long-time relaxation dynamics of spin systems. Such platforms have exquisite tunability of the global symmetries and dimensionality and are sufficiently well isolated from the environment such that magnon number and energy relaxing processes can be neglected.

II. MICROSCOPIC MODEL

We consider a Heisenberg ferromagnet in the presence of a Zeeman field and a small exchange anisotropy ϵ:

$$\hat{H} = -J \sum_{\langle jj' \rangle} \left(\hat{\boldsymbol{S}}_j \cdot \hat{\boldsymbol{S}}_{j'} + \epsilon \hat{S}^z_j \cdot \hat{S}^z_{j'} \right) + \Delta \sum_j \hat{S}^z_j. \tag{2}$$

Here j labels the lattice site, $\sum_{\langle jj' \rangle}$ denotes summation over nearest neighbors, and we take periodic boundary conditions in each spatial direction. We assume that the spin system has N lattice sites on a d dimensional cubical lattice, each containing a spin S degree of freedom which satisfies the commutation relations $[\hat{S}^z_j, \hat{S}^\pm_{j'}] = \pm \delta_{jj'} \hat{S}^\pm_j$ and $[\hat{S}^+_j, \hat{S}^-_{j'}] = 2\delta_{jj'} \hat{S}^z_j$, with $\hat{S}^\pm_j = \hat{S}^x_j \pm i\hat{S}^y_j$ as the raising and lowering spin operators. The Zeeman term plays an essential role experimentally because it gaps the spin-wave continuum and, for large Δ, it separates the magnon continuum from the gapless sound mode.

With the objective of deriving an effective model describing the low-energy manifold of $\hat{H}$, we recall that one magnon states $|\boldsymbol{k}\rangle = \hat{S}^+_{\boldsymbol{k}} |\mathrm{F}\rangle$, with $|\mathrm{F}\rangle = |\downarrow\downarrow \ldots \downarrow\rangle$ denoting the ferromagnetic ground state and $\hat{S}^+_{\boldsymbol{k}} = \frac{1}{\sqrt{N}} \sum_j e^{-i\boldsymbol{k}\cdot\boldsymbol{r}_j} \hat{S}^+_j$ are exact eigenstates of $\hat{H}$ with energies

$$\varepsilon_{\boldsymbol{k}} = \Delta + JS[\phi_0(1+\epsilon) - \phi_{\boldsymbol{k}}], \quad \phi_{\boldsymbol{k}} = \sum_{\boldsymbol{\tau} \in \mathrm{NN}} e^{i\boldsymbol{k}\cdot\boldsymbol{\tau}}. \tag{3}$$

Two magnon states $|\boldsymbol{k}, \boldsymbol{p}\rangle = \frac{1}{2S} \hat{S}^+_{\boldsymbol{k}} \hat{S}^+_{\boldsymbol{p}} |\mathrm{F}\rangle$, however, are *not* eigenstates of $\hat{H}$ [19,47,48]. Indeed, it is straightforward to show that

$$\hat{H}|\boldsymbol{k}, \boldsymbol{p}\rangle = (\varepsilon_{\boldsymbol{k}} + \varepsilon_{\boldsymbol{p}})|\boldsymbol{k}, \boldsymbol{p}\rangle + \frac{1}{N} \sum_{\boldsymbol{q}} g_{\boldsymbol{k},\boldsymbol{p},\boldsymbol{q}} |\boldsymbol{k}+\boldsymbol{q}, \boldsymbol{p}-\boldsymbol{q}\rangle,$$

$$g_{\boldsymbol{k},\boldsymbol{p},\boldsymbol{q}} = -J(\epsilon - \phi_{\boldsymbol{q}} + \phi_{\boldsymbol{q}-\boldsymbol{p}} + \phi_{\boldsymbol{q}+\boldsymbol{k}} - \phi_{\boldsymbol{k}+\boldsymbol{q}-\boldsymbol{p}}), \tag{4}$$

such that one magnon states are coupled via momentum-conserving collision $g_{\boldsymbol{k},\boldsymbol{p},\boldsymbol{q}}$. More generally, an N-magnon

state $\hat{H}|N\rangle = \hat{H}[\frac{1}{(2S)^{N/2}}\prod_i^N \hat{S}^+_{\boldsymbol{k}_i}]|F\rangle$ can also be decomposed into a diagonal component comprised of individual spin-wave energies and an off-diagonal component containing all possible combinations of two-body collisions. When the incoming magnons are close to the bottom of the band, the collision term is approximately $g_{\boldsymbol{k},\boldsymbol{p},\boldsymbol{q}} \approx -Ja^2(\epsilon + \boldsymbol{k}\cdot\boldsymbol{p})$. Importantly, whereas collisions between quasiparticles are hardcore in the easy axis/plane ferromagnet, collisions are soft under SU(2) symmetry ($\epsilon = 0$). We focus on the latter regime (for a discussion on the easy plane ferromagnet with broken U(1) symmetry, see Ref. [49]). We also note that $\epsilon = 0$ case is suitable for hydrodynamics in YIG if T is larger than dipolar energies [50], which is typically the case.

An effective description of the interacting magnon fluid which captures all the features of the parent SU(2) symmetric Hamiltonian in Eq. (2) is given by

$$\hat{H} = \int_{\boldsymbol{x}} \frac{\partial_\alpha \hat{\psi}^\dagger_{\boldsymbol{x}} \partial_\alpha \hat{\psi}_{\boldsymbol{x}}}{2m_0} + \frac{Ja^2}{4}(\hat{\psi}^\dagger_{\boldsymbol{x}}\hat{\psi}^\dagger_{\boldsymbol{x}}\partial_\alpha\hat{\psi}_{\boldsymbol{x}}\partial_\alpha\hat{\psi}_{\boldsymbol{x}} + \text{H.c.}), \quad (5)$$

where $m_0 = 1/2SJa^2$ is the magnon mass and $\hat{\psi}$ is a bosonic operator defined after a Holstein-Primakoff transformation ($\hat{S}^-_{\boldsymbol{x}} \approx \sqrt{2S}\hat{\psi}_{\boldsymbol{x}}$ and $\hat{S}^+_{\boldsymbol{x}} \approx \sqrt{2S}\hat{\psi}^\dagger_{\boldsymbol{x}}$), and summation over repeated indices is assumed. Equation (5) is valid in the dilute limit $na^d \ll S$ and small temperature $T \ll J$ such that only small momentum states are occupied.

III. MAGNON HYDRODYNAMICS WITHOUT GALILEAN SYMMETRY

The conserved quantities in Eq. (5) are $\hat{N} = \int_{\boldsymbol{x}} \hat{n}_{\boldsymbol{x}} = \int_{\boldsymbol{x}} \hat{\psi}^\dagger_{\boldsymbol{x}}\hat{\psi}_{\boldsymbol{x}}$, $\hat{P}_\alpha = \int_{\boldsymbol{x}} \hat{p}_{\alpha,\boldsymbol{x}} = \frac{-i}{2}\int_{\boldsymbol{x}} \hat{\psi}^\dagger_{\boldsymbol{x}}\partial_\alpha\hat{\psi}_{\boldsymbol{x}} - \text{H.c.}$, and $\hat{H}$. Although $\hat{P}_\alpha$ is not strictly conserved in the lattice model (2), it becomes conserved in the long-wavelength effective theory after neglecting Umklapp scattering. We use the *local equilibrium approximation* to describe the density matrix as $\hat{\rho} = \prod_{\boldsymbol{x}} \hat{\rho}_{\boldsymbol{x}}$, where space is coarse-grained into regions of size ℓ. The local-density matrix is $\hat{\rho}_{\boldsymbol{x}} = \exp(-\hat{H}/T - u_\alpha\hat{P}_\alpha - \mu\hat{N})_{\boldsymbol{x}}$, with $(T, u_\alpha, \mu)_{\boldsymbol{x}}$ the position and time-dependent thermodynamic potentials. One important aspect of Eq. (5) is that the particle current operator, defined as $\partial_\alpha\hat{J}_\alpha = -i[\hat{H}, \hat{n}_{\boldsymbol{x}}]$, is *not equal* to $\hat{P}_\alpha$; instead, $\hat{J}_\alpha$ takes the form $\hat{J}_\alpha = \hat{P}_\alpha/m_0 + \frac{iJa^2}{2}(\hat{\psi}^\dagger_{\boldsymbol{x}}\hat{\psi}^\dagger_{\boldsymbol{x}}\hat{\psi}_{\boldsymbol{x}}\partial_\alpha\hat{\psi}_{\boldsymbol{x}} - \text{H.c.})$ and gives rise to Galilean symmetry breaking. As such, a variety of interesting effects emerge, including velocity-dependent transport coefficients, anomalous viscous terms, and anisotropic dispersion of hydrodynamic fluctuations, to name a few.

To make analytical progress, we compute expectation values using a Gaussian approximation of the distribution function $\rho_{\boldsymbol{x}}$ which can be formally implemented by using $\hat{H}/T \approx \sum_{\boldsymbol{k}} \frac{\boldsymbol{k}^2}{2mT}\hat{\psi}^\dagger_{\boldsymbol{k}}\hat{\psi}_{\boldsymbol{k}}$, with m the renormalized magnon mass. As such, any N-point correlation functions can be expressed as products of two point correlation functions. Because corrections to the bare mass are small, $\delta m = m - m_0 \sim \mathcal{O}(na^2T/J) \ll 1$, below we will use m and m_0 interchangeably. The expectation values of conserved quantities ($\langle\hat{N}\rangle_{\boldsymbol{x}} = n$, $\langle\hat{P}_\alpha\rangle_{\boldsymbol{x}} = np_\alpha$, $\langle\hat{H}\rangle_{\boldsymbol{x}} = n\varepsilon$) are given by

$$n = \frac{mT}{2\pi}g_1(z), \quad p_\alpha = mu_\alpha, \quad \theta = \frac{Tg_2(z)}{g_1(z)}, \quad (6)$$

where the thermal energy θ is related to energy density through $\varepsilon = \theta + \frac{(1-na^2/4S)p^2}{2m}$, and where we assumed a 2D system. In Eq. (6), $z = e^{-\mu/T}$ is the fugacity, and $g_q(z)$ is the Bose integral, $g_q(z) = \frac{1}{\Gamma(q)}\int_0^\infty \frac{dy y^{q-1}}{e^y/z-1}$[$\Gamma(q)$: Gamma function].

The particle current J_α, the momentum current $\Pi_{\alpha\beta} = \langle\hat{\Pi}_{\alpha\beta}\rangle$, and the energy current $Q_\alpha = \langle\hat{Q}_\alpha\rangle$ are given by

$$\begin{aligned} J_\alpha &= nv_\alpha, \\ \Pi_{\alpha\beta} &= np_\alpha v_\beta + P_{\alpha\beta}, \\ Q_\alpha &= n\varepsilon v_\alpha + P_{\alpha\beta}v_\beta + q_\alpha; \end{aligned} \quad (7)$$

see details in Appendix B. Here $P_{\alpha\beta} = (n\theta - \frac{\gamma np^2}{2m})\delta_{\alpha\beta} + \tilde{P}_{\alpha\beta}$ is the pressure tensor, $\tilde{P}_{\alpha\beta}$ is the dissipative (viscous) component, and q_α is the heat current (both $\tilde{P}_{\alpha\beta}$ and q_α will be defined explicitly below). The main consequence of Galilean symmetry breaking in our work is that conserved quantities flow with a drift velocity $v_\alpha = \langle\hat{J}_\alpha\rangle/n$ which is different from the thermodynamic potential u_α:

$$v_\alpha = (1-\gamma)u_\alpha, \quad \gamma = \frac{na^2}{S}. \quad (8)$$

The continuity equations for each of the conserved charges lead to the hydrodynamic equations:

$$\begin{aligned} &\dot{n} + \partial_\alpha(nv_\alpha) = 0, \\ &\dot{p}_\alpha + v_\beta\partial_\beta p_\alpha = -\frac{1}{n}\partial_\beta P_{\alpha\beta}, \\ &\dot{\theta} + v_\alpha\partial_\alpha\theta = -\frac{1}{n}\partial_\alpha q_\alpha - \frac{1}{n}P_{\alpha\beta}\partial_\alpha v_\beta - \gamma\frac{p^2}{2m}\partial_\alpha v_\alpha, \end{aligned} \quad (9)$$

which resemble usual hydrodynamic equations for a classical fluid with the caveat that convective terms contain v_α rather than u_α. We recall that the "single fluid" equations (9) do not include dynamics of the condensate due to the zero coupling with $\boldsymbol{k} = 0$ modes in the SU(2) symmetric Hamiltonian.

IV. DISSIPATIVE EFFECTS

We incorporate dissipation effects phenomenologically using the relaxation time approximation; see Appendix C. This approximation allows us to relate the nonequilibrium magnon distribution to gradients in $\eta_j = (n, u_\alpha, \theta)$, i.e., $n_{\boldsymbol{k}} = \bar{n}_{\boldsymbol{k}} + \tau_{\boldsymbol{k}}\sum_j(\partial\bar{n}_{\boldsymbol{k}}/\partial\eta_j)(\partial_t + \boldsymbol{v}_{\boldsymbol{k}}\cdot\nabla_{\boldsymbol{r}})\eta_j$, where $\tau_{\boldsymbol{k}}$ is a momentum-dependent relaxation time. As a result, $\tilde{P}_{\alpha\beta}$ and q_α can be written $\tilde{P}_{\alpha\beta} = \nu(\partial_\alpha u_\beta + \partial_\beta u_\alpha - \delta_{\alpha\beta}\partial_\gamma u_\gamma)$, and $q_\alpha = \kappa_n\partial_\alpha n + \kappa_\theta\partial_\alpha\theta$. For a 2D magnon gas with quadratic dispersion and collision rate of the form $1/\tau_{\boldsymbol{k}} \propto \boldsymbol{k}^2$, we find that, within the relaxation time approximation, dissipation is dominated by viscous effects with scaling $\nu \sim \frac{J^2}{T}$. While we will keep track of κ_n and κ_θ in our equations of motion, we set $\kappa_n = \kappa_\theta = 0$ in the numerics.

V. HYDRODYNAMIC MODES

The sound mode originates from the longitudinal spin fluctuations and is manifested in the retarded correlator

$$\chi_{zz}(\boldsymbol{q},\omega) = -i\int_0^\infty dt e^{i\omega t}\sum_\tau e^{-i\boldsymbol{q}\cdot\boldsymbol{\tau}}\langle[\hat{S}^z_i(t), \hat{S}^z_{i+\tau}(0)]\rangle. \quad (10)$$

This is equivalent to computing density fluctuation because $\hat{S}_i^z = -S(1-\hat{n}_i)$. With this objective in mind, we first linearize Eq. (9) around the equilibrium values, $n(\boldsymbol{r},t) = \bar{n} + \delta n(\boldsymbol{r},t)$, $\theta(\boldsymbol{r},t) = \bar{\theta} + \delta\theta(\boldsymbol{r},t)$, and $v_\alpha(\boldsymbol{r},t) = \delta v_\alpha(\boldsymbol{r},t)$ and go to momentum space:

$$\mathbb{A}\begin{pmatrix}\delta n\\ \delta v_\parallel\\ \delta\theta\end{pmatrix} = \begin{pmatrix}0\\ iF_\parallel/m\\ 0\end{pmatrix},$$
$$\mathbb{A} = \begin{pmatrix}\omega & -\bar{n}q & 0\\ -\bar{\theta}q/m\bar{n} & \omega/(1-\gamma)+i\nu q^2/\bar{n} & -q/m\\ -i\kappa_n q^2/\bar{n} & -\bar{\theta}q & \omega - i\kappa_\theta q^2/\bar{n}\end{pmatrix}. \tag{11}$$

The coupling between δn, $\delta v_\parallel$ and $\delta\theta$ gives rise to two propagating modes and one diffusive mode. The transverse momentum component, $\delta u_\perp$, which does not couple to δn, gives rise to an extra diffusive mode, $(\omega + i\nu q^2/\bar{n})\delta v_\perp = iF_\perp/m$. Here we included in our equations a fluctuating parallel (transverse) force $F_\parallel$ ($F_\perp$). Close to thermal equilibrium, the density–density correlation function can be obtained from Eq. (11) using the fluctuation-dissipation theorem:

$$\chi_{zz}(q,\omega) = \frac{JS^2(\bar{n}qa^2)^2}{\omega^2/(1-\gamma) - \zeta(q,\omega)\bar{\theta}q^2/m + i\nu\omega q^2/\bar{n}}, \tag{12}$$

where $\zeta(q,\omega) = 1 + \frac{\omega - i\kappa_n q^2/\bar{\theta}}{\omega + i\kappa_\theta q^2/\bar{n}} \approx 2$ at the intermediate/large frequency range of interest. In this regime, the response function exhibits a linearly dispersing sound mode $\omega = v_s q$, with $v_s = a\sqrt{2(1-\gamma)J\theta}$; see Fig. 1.

VI. DETECTION OF THE SOUND MODE

We consider a spin-1/2 qubit with an intrinsic level splitting ω placed a distance d above the thin magnetic insulator. The combined dynamics of the qubit and ferromagnet are governed by the Hamiltonian $\hat{H}_{\text{total}} = \hat{H} + \hat{H}_c + \hat{H}_q$, where $\hat{H}_q$ is the spin qubit Hamiltonian $\hat{H}_q = \frac{1}{2}\omega\sigma_z$ with the polarizing field assumed to be aligned in the z direction. The term $\hat{H}_c$ is the qubit-ferromagnet coupling induced by dipole–dipole interactions:

$$\hat{H}_c = \frac{\mu_B^2}{2}\hat{\boldsymbol{\sigma}}\cdot\hat{\boldsymbol{B}}, \quad \hat{\boldsymbol{B}} = \frac{1}{4\pi}\sum_j\left[\frac{\hat{\boldsymbol{S}}_j}{r_j^3} - \frac{3(\hat{\boldsymbol{S}}_j\cdot\boldsymbol{r}_j)\boldsymbol{r}_j}{r_j^5}\right], \tag{13}$$

where $\boldsymbol{r}_j = (x_j, y_j, -d)$ is the relative position between the i-th spin in the 2D lattice and probe. The relaxation time of the spin qubit can be obtained from Fermi Golden's rule $1/T_1 = \frac{\mu_B^2}{2}\int_{-\infty}^{\infty} dt e^{i\omega t}\langle\{\hat{B}^-(t), \hat{B}^+(0)\}\rangle$, where $\{,\}$ denotes anticommutation (see Appendix D). Replacing Eq. (13) into $1/T_1$ and using the fluctuation-dissipation theorem, the relaxation time can be expressed in terms of spin-correlation functions:

$$\frac{1}{T_1} = \coth\left(\frac{\omega}{2T}\right)\frac{\mu_B^2}{2a^2}\int\frac{d^2\boldsymbol{q}}{(2\pi)^2}e^{-2|\boldsymbol{q}|d}|\boldsymbol{q}|^2[\chi''_{-+}(\boldsymbol{q},\omega) + \chi''_{+-}(\boldsymbol{q},\omega) + 4\chi''_{zz}(\boldsymbol{q},\omega)], \tag{14}$$

where we denote $\chi''_{\alpha\beta} = -\text{Im}[\chi_{\alpha\beta}]$, and $\chi^R_{\alpha\beta}(\boldsymbol{q},\omega) = -i\int_0^\infty dt\langle[\hat{S}^\alpha_{-\boldsymbol{q}}(t), \hat{S}^\beta_{\boldsymbol{q}}(0)]\rangle$. Figure 1 shows the integrand of Eq. (14), and Fig. 2 shows the spin-relaxation time as a function of ω induced by longitudinal and transverse spin fluctuations (we assumed a constant magnon population $\bar{n}$ and T). The correlators $\chi_{\pm\mp}(\boldsymbol{q},\omega)$ are related to single-magnon production/absorption, which we assume to be given by $\chi^{-1}_{+-}(\boldsymbol{q},\omega) = \omega - \omega_{\boldsymbol{q}} + i\Sigma''(\boldsymbol{q},\omega)$, where $\Sigma''(\boldsymbol{q},\omega) \sim \frac{T\omega}{J}(qa)^2$ (valid for $z \sim 1$ and $\omega \ll T$) is the imaginary part of the self-energy computed from the bubble diagram; see inset of Fig. 2 and details in Appendix E. We also note that, in Fig. 2, we normalize $1/T_1$ with $\coth(\omega/2T)$ to capture the spectral contribution of spin fluctuations rather than its amplitude. Figure 2 is the main result of this work and shows a clear fingerprint of the sound mode within the gap of the ferromagnet.

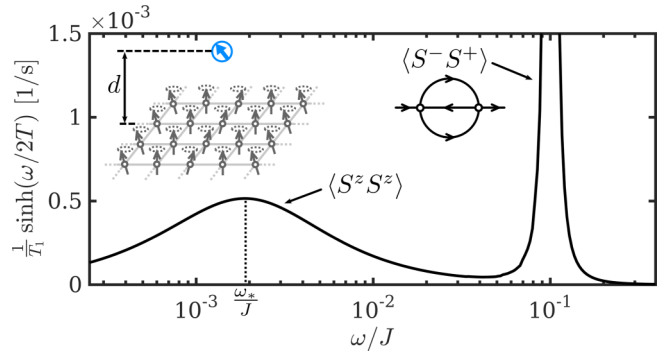

FIG. 2. Relaxation time [normalized by $\sinh(\omega/2T)$] of a spin qubit located a distance d from the 2D ferromagnet. Besides the characteristically large relaxation rate induced by spin relaxation due to emission of spin waves at energy Δ, the relaxation rate exhibits a peak below the ferromagentic gap induced by emission of sound modes with velocity v_s. Parameters used: $na^2 = 0.03$, $T/J = 0.2$, $\Delta/J = 0.1$, $a = 0.3$ nm, and $d = 20$ nm.

VII. DIPOLAR INTERACTIONS

Contrary to classical and electron fluids where particles cannot be created or annihilated, conservations laws are not as robust in a magnon fluid and therefore should be subject to scrutiny. Dipolar interactions lead to magnon decay via three-magnon processes, particularly in thin layers with a canted ferromagnetic order parameter. Assuming a magnon distribution with $z < 1$, we estimate the typical magnon decay time induced by a dipolar term $\hat{H}_d = \frac{g_d}{2}\sum_{jj'}[\frac{\hat{\boldsymbol{S}}_j\cdot\hat{\boldsymbol{S}}_{j'}}{r^3_{jj'}} - \frac{3(\hat{\boldsymbol{S}}_j\cdot\boldsymbol{r}_{jj'})(\hat{\boldsymbol{S}}_{j'}\cdot\boldsymbol{r}_{jj'})}{r^5_{jj'}}]$, with $g_d = \mu_B^2/4\pi$. As shown in Appendix F, this gives values in the ballpark $\frac{1}{\bar{n}}\frac{d\bar{n}}{dt} \sim \frac{g_d^2}{J}(z^2 - z^3) \sim$ MHz, several orders of magnitude smaller than the typical GHz frequencies that typical spin qubit magnetometers can access. As a result, sound modes are expected to be well-defined excitations in a wide range of frequencies from MHz to several GHz.

VIII. CONCLUSION

Our model and theoretical predictions, which are relevant to ongoing experiments using spin qubit magnetometers on ferromagnetic insulators and in cold atomic gases, provide distinct signatures of hydrodynamic behavior in spin

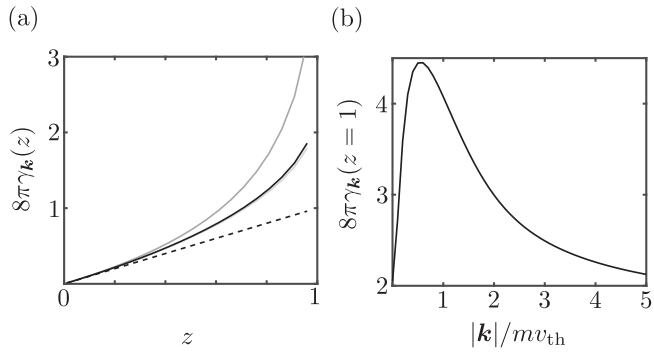

FIG. 3. (a) $\gamma_{\boldsymbol{k}}(z)$ plotted for different values $|\boldsymbol{k}|/mv_{\rm th} = 0, 1, 5$ (increasing darkness). Indicated with a dashed line is the linear $\gamma_{\boldsymbol{k}}(z) = z/8\pi$ obtained from the classical Boltzmann equation. (b) $\gamma_{\boldsymbol{k}}(z)$ exhibits a weak dependence on k, as shown for $z = 1$. At most, $\gamma_{\boldsymbol{k}}(z)$ varies by a factor of $\sim$2.5 as k is varied. In our calculations, we take the average of $\gamma_{\boldsymbol{k}}$ over $\boldsymbol{k}$ space.

systems. Although the sound mode is its most distinctive feature, the strong momentum dependence of the magnon–magnon interaction induced by the SU(2) symmetry suggests that ferromagnets can also host anomalous transport not achievable in classical and electron fluids.

ACKNOWLEDGMENTS

We acknowledge useful discussions with D. Abanin, T. Andersen, S. Chernyshev, C. Du, M. D. Lukin, A. Rosch, D. Sels, A. Yacoby, J. Sanchez-Yamagishi, and T. Zhou. J.F.R.-N. and E.D. acknowledge support from Harvard-MIT CUA, AFOSR-MURI: Photonic Quantum Matter (Award No. FA95501610323), DARPA DRINQS program (Award No. D18AC00014). D.P. thanks support by the Joint UGS-ISF Research Grant Program under Grant No. 1903/14 and by the National Science Foundation through a grant to ITAMP at the Harvard-Smithsonian Center for Astrophysics.

APPENDIX A: RELAXATION TIME DUE TO EXCHANGE COUPLING

To estimate the relaxation time induced by the exchange interaction, we consider a magnon fluid at thermodynamic equilibrium and zero drift velocity, $\bar{n}_{\boldsymbol{k}} = 1/(z^{-1}e^{\varepsilon_{\boldsymbol{k}}/T} - 1)$. Let us assume that, at $t = 0$, a nonequilibrium distribution is formed with a bump at wave-vector $\boldsymbol{k}$, i.e., $n_{\boldsymbol{p}} = \bar{n}_{\boldsymbol{p}} + \delta n_{\boldsymbol{k}}\delta_{\boldsymbol{k},\boldsymbol{p}}$. The relaxation time for such a distribution is given by

$$\frac{1}{\tau_{\boldsymbol{k}}} = \frac{(Ja^2)^2}{N^2}\sum_{\boldsymbol{pq}}(\boldsymbol{k}\cdot\boldsymbol{p})^2 2\pi\delta(\varepsilon_{\boldsymbol{k}} + \varepsilon_{\boldsymbol{p}} - \varepsilon_{\boldsymbol{k}+\boldsymbol{q}} - \varepsilon_{\boldsymbol{p}-\boldsymbol{q}}) \times [\bar{n}_{\boldsymbol{p}}(1+\bar{n}_{\boldsymbol{k}+\boldsymbol{q}})(1+\bar{n}_{\boldsymbol{p}-\boldsymbol{q}}) - (1+\bar{n}_{\boldsymbol{p}})\bar{n}_{\boldsymbol{k}+\boldsymbol{q}}\bar{n}_{\boldsymbol{p}-\boldsymbol{q}}]. \tag{A1}$$

The relaxation time can be expressed as $\frac{1}{\tau_{\boldsymbol{k}}} = \frac{\gamma_{\boldsymbol{k}}(z)}{16\pi}\frac{T^2(ka)^2}{J}$ after factoring out the $\boldsymbol{k}$ vector dependence out of the integral, normalizing energies with T, and momenta with $\sqrt{2mT}$. The dimensionless prefactor $\gamma_{\boldsymbol{k}}(z)$ is plotted in Fig. 3, exhibits a weak dependence on $\boldsymbol{k}$, and scales approximately as $\propto z$. Rather than keeping this unimportant $\boldsymbol{k}$ dependence of $\gamma_{\boldsymbol{k}}$, we define an average γ of all $\boldsymbol{k}$ vectors and z values, $\gamma(z)/z = \int_0^1 dz/z \int d^2\tilde{\boldsymbol{k}}/(2\pi)^2\gamma_{\boldsymbol{k}}(z)$, which yields $\gamma(z) \approx cz$, with $c \sim \mathcal{O}(1)$.

In thermal equilibrium, the typical relaxation rate for thermal magnons is given by $1/\bar{\tau} \sim \frac{T^2(na^2)}{J}$. The relaxation length of thermal magnons is given by $\ell = \bar{v}\bar{\tau}$, where $\bar{v}^2 = \frac{1}{2\pi mn}\int_0^\infty dk k^3\bar{n}_{\boldsymbol{k}} = 2mTg_2(z)/g_1(z)$ is the thermal velocity and results in Eq. (1) of the main text.

APPENDIX B: DERIVATION OF HYDRODYNAMIC EQUATIONS

In this section we derive the current operators associated with the conserved quantities of the effective Hamiltonian

$$\hat{H} = \int_{\boldsymbol{x}} \frac{\partial_\alpha\hat{\psi}^\dagger_{\boldsymbol{x}}\partial_\alpha\hat{\psi}_{\boldsymbol{x}}}{2m} + g(\hat{\psi}^\dagger_{\boldsymbol{x}}\hat{\psi}^\dagger_{\boldsymbol{x}}\partial_\alpha\hat{\psi}_{\boldsymbol{x}}\partial_\alpha\hat{\psi}_{\boldsymbol{x}} + \text{H.c.}), \tag{B1}$$

which was derived in the main text. Here we defined $g = Ja^2/4$ for compactness of notation. We recall that the Hamiltonian (B1) has three conserved quantities: Particle number $\hat{N} = \int_{\boldsymbol{x}}\hat{n}_{\boldsymbol{x}} = \int_{\boldsymbol{x}}\hat{\psi}^\dagger_{\boldsymbol{x}}\hat{\psi}_{\boldsymbol{x}}$, momentum $\hat{P}_\alpha = \int_{\boldsymbol{x}}\hat{p}_{\alpha,\boldsymbol{x}} = \frac{-i}{2}\int_{\boldsymbol{x}}\hat{\psi}^\dagger_{\boldsymbol{x}}\partial_\alpha\hat{\psi}_{\boldsymbol{x}} -$ H.c., and energy $\hat{H} = \int_{\boldsymbol{x}}\hat{\epsilon}_{\boldsymbol{x}}$. We proceed to derive the currents associated with each of the conserved quantities.

1. Current operators

The current operators can be derived from the continuity relation that ensures charge conservation: $\partial_t\hat{n}_{\boldsymbol{x}} = -\partial_\alpha\hat{J}_\alpha = i[\hat{H}, \hat{n}_{\boldsymbol{x}}]$ for particle number, $\partial_t\hat{p}_{\alpha,\boldsymbol{x}} = -\partial_\alpha\hat{\Pi}_{\alpha,\beta} = i[\hat{H}, p_{\beta,\boldsymbol{x}}]$ for momentum, and $\partial_t\hat{\epsilon}_{\boldsymbol{x}} = -\partial_\alpha\hat{Q}_\alpha = i[\hat{H}, \hat{\epsilon}_{\boldsymbol{x}}]$ for energy. Computing the commutator of $\hat{H}$ with each of the local operators gives rise to the currents:

$$\begin{aligned}
\hat{J}_\alpha &= \frac{-i}{2m}[\hat{\psi}^\dagger_{\boldsymbol{x}}\partial_\alpha\hat{\psi}_{\boldsymbol{x}} - \text{H.c.}] + 2ig[\hat{\psi}^\dagger_{\boldsymbol{x}}\hat{\psi}^\dagger_{\boldsymbol{x}}\partial_\alpha\hat{\psi}_{\boldsymbol{x}}\hat{\psi}_{\boldsymbol{x}} - \text{H.c.}],\\
\hat{\Pi}_{\alpha\beta} &= \frac{1}{2m}[\partial_\alpha\hat{\psi}^\dagger_{\boldsymbol{x}}\partial_\beta\hat{\psi}_{\boldsymbol{x}} + \text{H.c.}] + g[(\hat{\psi}_{\boldsymbol{x}}\partial_\gamma\hat{\psi}_{\boldsymbol{x}})^2\delta_{\alpha\beta} + 2\hat{\psi}^\dagger_{\boldsymbol{x}}\hat{\psi}^\dagger_{\boldsymbol{x}}\partial_\alpha\hat{\psi}_{\boldsymbol{x}}\partial_\beta\hat{\psi}_{\boldsymbol{x}} + \text{H.c.}],\\
\hat{Q}_\alpha &= \frac{-i}{4m}[\partial_\beta\hat{\psi}^\dagger_{\boldsymbol{x}}\partial_\alpha\partial_\beta\hat{\psi}_{\boldsymbol{x}} - \text{H.c.}] - \frac{ig}{m}[\hat{\psi}^\dagger_{\boldsymbol{x}}\hat{\psi}^\dagger_{\boldsymbol{x}}\partial_\beta\hat{\psi}_{\boldsymbol{x}}\partial_\alpha\partial_\beta\hat{\psi}_{\boldsymbol{x}} + \hat{\psi}^\dagger_{\boldsymbol{x}}\hat{\psi}^\dagger_{\boldsymbol{x}}\partial_\alpha\hat{\psi}_{\boldsymbol{x}}\partial^2_\beta\hat{\psi}_{\boldsymbol{x}} - \partial_\alpha\hat{\psi}^\dagger_{\boldsymbol{x}}\hat{\psi}^\dagger_{\boldsymbol{x}}\partial_\beta\hat{\psi}_{\boldsymbol{x}}\partial_\beta\hat{\psi}_{\boldsymbol{x}} - \text{H.c.}].
\end{aligned} \tag{B2}$$

2. Currents within the Gaussian approximation

We compute the expectation value of the currents using the *local equilibrium* approximation which allows us to coarse-grain real space in regions of size ℓ in which the system is effectively thermalized. We also employ the Gaussian approximation to represent the density matrix in the subregion

region $\boldsymbol{x}$ as $\hat{\rho}_{\boldsymbol{x}} = \exp(-\sum_{\boldsymbol{k}} \frac{\boldsymbol{k}^2}{2mT}\psi^\dagger_{\boldsymbol{k}}\psi_{\boldsymbol{k}} - u_\alpha \hat{P}_\alpha - \mu\hat{N})$, where we use the bare mass m rather than the renormalized mass for simplicity. The Gaussian approximation enables us to compute four-point correlation functions in terms of two-point correlations function. In particular, the expectation value of the currents is given by

$$
\begin{aligned}
n = \langle 1\rangle \quad J_\alpha &= \frac{\langle k_\alpha\rangle}{m} - 8g\langle 1\rangle\langle k_\alpha\rangle,\\
P_\alpha = \langle k_\alpha\rangle, \quad \Pi_{\alpha\beta} &= \frac{\langle k_\alpha k_\beta\rangle}{m} - 4g\langle k_\gamma\rangle\langle k_\gamma\rangle\delta_{\alpha\beta} - 8g\langle k_\alpha\rangle\langle k_\beta\rangle,\\
\epsilon &= \frac{\langle k_\beta k_\beta\rangle}{2m} - 4g\langle k_\beta\rangle\langle k_\beta\rangle,\\
Q_\alpha &= \frac{\langle k_\alpha k_\beta k_\beta\rangle}{2m^2} - 8g\langle k_\beta\rangle\frac{\langle k_\alpha k_\beta\rangle}{m} - 4g\langle k_\alpha\rangle\frac{\langle k_\beta k_\beta\rangle}{m},
\end{aligned}
\tag{B3}
$$

where we used the short-hand notations $\langle A\rangle = \int \frac{d\boldsymbol{k}}{(2\pi)^2} A_{\boldsymbol{k}} n_{\boldsymbol{k}}$, and $n_{\boldsymbol{k}}$ is the Bose distribution function with chemical potential μ, drift velocity u_α, and temperature T. It is straightforward to compute the expectation values, which are given by $\langle 1\rangle = mTg_1(z)/2\pi$, $\langle k_\alpha\rangle = nmu_\alpha$, $\langle k_\alpha k_\beta\rangle = mnu_\alpha u_\beta + \langle \tilde{k}_\alpha\tilde{k}_\beta\rangle$, and $\langle k_\alpha k_\beta k_\beta\rangle = \langle \tilde{k}_\alpha\tilde{k}_\beta\tilde{k}_\beta\rangle + mu_\alpha\langle\tilde{k}_\beta\tilde{k}_\beta\rangle + 2mu_\beta\langle\tilde{k}_\alpha\tilde{k}_\beta\rangle + m^3nu^2u_\alpha$ [here $g_\nu(z)$ is the Bose integral defined in the main text, $\tilde{k}_\alpha = k_\alpha - mu_\alpha$, and we used $d = 2$]. The term $\langle\tilde{k}_\alpha\tilde{k}_\beta\rangle = P_{\alpha\beta} = n\theta\delta_{\alpha\beta} + P'_{\alpha\beta}$ is the pressure tensor, $P'_{\alpha\beta}$ is the dissipative component, and $\langle\tilde{k}_\alpha\tilde{k}_\beta\tilde{k}_\beta\rangle = q_\alpha$ is the heat current. Both $P'_{\alpha\beta}$ and q_α are estimated below. Replacing the expectation values into Eq. (B3) results in the charges and currents:

$$
\begin{aligned}
n, J_\alpha &= nv_\alpha,\\
p_\alpha &= mu_\alpha, \quad \Pi_{\alpha\beta} = P_{\alpha\beta} + np_\alpha v_\beta,\\
\epsilon &= \frac{d\theta}{2} + \frac{p_\alpha v_\beta}{2}, \quad Q_\alpha = q_\alpha + n\epsilon v_\alpha + P_{\alpha\beta}v_\beta.
\end{aligned}
\tag{B4}
$$

The continuity equations $\partial n + \partial_\alpha J_\alpha = 0$, $\partial_t(np_\alpha) + \partial_\beta\Pi_{\alpha\beta} = 0$, and $\partial_t(n\epsilon) + \partial_\alpha Q_\alpha = 0$ give rise to the hydrodynamic equations (9) in the main text.

APPENDIX C: ESTIMATING TRANSPORT COEFFICIENTS FROM THE RELAXATION TIME APPROXIMATION

To compute the leading-order corrections to $P_{\alpha\beta}$ and q_α, we need to determine $\delta n_{\boldsymbol{k}}$ induced by gradients in n, u_α, and θ. With this objective in mind, we linearize the Boltzmann kinetic equation

$$
(\partial_t + v_{\boldsymbol{k},\alpha}\partial_\alpha + F_\alpha\partial_{k_\alpha})\bar{n}_{\boldsymbol{k}} = I(\bar{n}_{\boldsymbol{k}} + \delta n_{\boldsymbol{k}}). \tag{C1}
$$

Here we assumed that $\delta n_{\boldsymbol{k}} \ll n_{\boldsymbol{k}}$, such that the leading-order contributions on the left-hand side is given by the derivatives (both space and time) of $\bar{n}_{\boldsymbol{k}}$. The right-hand side is already leading order in $\delta n_{\boldsymbol{k}}$ because $I(\bar{n}_{\boldsymbol{k}}) = 0$.

We begin the analysis by considering the left-hand side of Eq. (C1). We recall that $\bar{n}_{\boldsymbol{k}}(n, u_\alpha, \theta)$ is the local distribution function which depends implicitly on n, u_α, and θ. As such, computing the time and spatial derivatives of $\bar{n}_{\boldsymbol{k}}$ leads to

$$
[\partial_t + v_{\boldsymbol{k},\alpha}\partial_\alpha]\bar{n}_{\boldsymbol{k}} = [\dot{n} + v_{\boldsymbol{k},\alpha}\partial_\alpha n]\partial_n\bar{n}_{\boldsymbol{k}}|_{\theta,u_\alpha} + [\dot{\theta} + v_{\boldsymbol{k},\alpha}\partial_\alpha\theta]\partial_\theta\bar{n}_{\boldsymbol{k}}|_{n,u_\alpha} + [\dot{u}_\alpha + v_{\boldsymbol{k},\beta}\partial_\beta u_\alpha]\partial_{u_\alpha}\bar{n}_{\boldsymbol{k}}|_{n,\theta}, \tag{C2}
$$

where $\partial\bar{n}_{\boldsymbol{k}}/\partial x|_{y,z}$ denotes the derivative of $\bar{n}_{\boldsymbol{k}}$ with respect to x, leaving y and z constant. In Eq. (C2), we replace the time derivatives $\dot{n}$, $\dot{u}_\alpha$, and $\dot{\theta}$ by the hydrodynamic equations (9) of the main text in the local equilibrium approximation and compute transport coefficients to leading order in na^2 and in, i.e., using $P_{\alpha\beta} = \delta_{\alpha\beta}n\theta/m$ and $q_\alpha = 0$. This results in

$$
\begin{aligned}
[\partial_t + v_{\boldsymbol{k},\alpha}\partial_\alpha + F_\alpha\partial_{k_\alpha}]\bar{n}_{\boldsymbol{k}} = &\left[\delta_{\alpha\beta}\partial_n\bar{n}_{\boldsymbol{k}}\Big|_{\theta,u_\alpha} + \frac{m}{n}\partial_n P_{\alpha\beta}\partial_{\theta_{\boldsymbol{k}}}\bar{n}_{\boldsymbol{k}}\right]\tilde{v}_{\boldsymbol{k},\beta}\partial_\alpha n + [\delta_{\alpha\beta}\partial_\theta\bar{n}_{\boldsymbol{k}}|_{n,u_\alpha} + \frac{m}{n}\partial_\theta P_{\alpha\beta}\partial_{\theta_{\boldsymbol{k}}}\bar{n}_{\boldsymbol{k}}]\tilde{v}_{\boldsymbol{k},\beta}\partial_\alpha\theta\\
&-\left[\delta_{\alpha\beta}n\partial_n\bar{n}_{\boldsymbol{k}}\Big|_{\theta,u_\alpha} + \frac{m}{n}P_{\alpha\beta}\partial_\theta\bar{n}_{\boldsymbol{k}}\Big|_{n,u_\alpha} + m\tilde{v}_{\boldsymbol{k},\alpha}\tilde{v}_{\boldsymbol{k},\beta}\partial_{\theta_{\boldsymbol{k}}}\bar{n}_{\boldsymbol{k}}\right]\partial_\alpha u_\beta,
\end{aligned}
\tag{C3}
$$

where we used the identities $\partial\bar{n}_{\boldsymbol{k}}/\partial u_\alpha|_{n,\theta} = -[\partial\bar{n}_{\boldsymbol{k}}/\partial\theta_{\boldsymbol{k}}]m\tilde{v}_{\boldsymbol{k},\alpha}$ and $F_\alpha\partial_{k_\alpha}\bar{n}_{\boldsymbol{k}} = F_\alpha[\partial\bar{n}_{\boldsymbol{k}}/\partial\theta_{\boldsymbol{k}}]\tilde{v}_{\boldsymbol{k},\alpha}$. The terms in brackets in Eq. (C3) are thermodynamic functions that depend on the local values of T, z, w_α and are given by

$$
\begin{aligned}
[\partial_t + v_{\boldsymbol{k},\alpha}\partial_\alpha + F_\alpha\partial_{k_\alpha}]\bar{n}_{\boldsymbol{k}} = &\left[\frac{2\pi}{mT}\left(h_n(z) + \tilde{h}_n(z)\frac{\theta_{\boldsymbol{k}}}{T}\right)\tilde{v}_{\boldsymbol{k},\alpha}\partial_\alpha n + \frac{2\pi}{T}\left(h_\theta(z) + \tilde{h}_\theta(z)\frac{\theta_{\boldsymbol{k}}}{T}\right)\tilde{v}_{\boldsymbol{k},\alpha}\partial_\alpha\theta\right.\\
&\left.+\left(\delta_{\alpha\beta}\frac{\theta_{\boldsymbol{k}}}{T} - \frac{mv_{\boldsymbol{k},\alpha}v_{\boldsymbol{k},\beta}}{T}\right)\partial_\alpha u_\beta\right]\bar{n}_{\boldsymbol{k}}(\bar{n}_{\boldsymbol{k}} + 1),
\end{aligned}
\tag{C4}
$$

where the dimensionless coefficients $h_{n,\theta}(z)$ and $\tilde{h}_{n,\theta}(z)$ are

$$
\begin{aligned}
h_n(z) &= \frac{zg_2^2 - (1-z)g_2g_1^2}{zg_2g_1^2 - (1-z)g_1^4/2}, \quad \tilde{h}_n(z) = \left[\frac{1}{g_1} + \frac{zg_2}{g_1^2(1-z) - 2zg_2}\right],\\
h_\theta(z) &= \frac{zg_2^2 - (1-z)g_2g_1^2}{zg_2g_1^2 - (1-z)g_1^4/2}, \quad \tilde{h}_\theta(z) = \left[\frac{1}{g_1} + \frac{zg_2}{g_1^2(1-z) - 2zg_2}\right].
\end{aligned}
\tag{C5}
$$

Let us now focus on the right-hand side of Eq. (C1). There are many schemes to calculate $I[\bar{n}_{\boldsymbol{k}} + \delta n_{\boldsymbol{k}}]$. The simplest approach is to use the *relaxation time approximation*. In this approximation, the collision integral is written as $I[\bar{n}_{\boldsymbol{k}} +$

$\delta n_{\boldsymbol{k}}] \approx -\delta n_{\boldsymbol{k}}/\tau_{\boldsymbol{k}}$, where $\tau_{\boldsymbol{k}}$ is defined in Eq. (A1). Importantly, we keep the explicit dependence on the magnon wave vector. We note that $1/\tau_{\boldsymbol{k}}$ was calculated using $u_\alpha = 0$, but its value remains valid so long as $u_\alpha \lesssim \sqrt{T/m}$ [corrections to $1/\tau_{\boldsymbol{k}}$ due to finite drift velocity are $O(u_\alpha^2)$]. As a result, $\delta n_{\boldsymbol{k}}$ becomes proportional to gradients in n, θ, and u_α:

$$\begin{aligned}\delta n_{\boldsymbol{k}} = \tau_{\boldsymbol{k}}\Bigg[&\frac{2\pi}{mT}\left(h_n(z)+\tilde{h}_n(z)\frac{\theta_{\boldsymbol{k}}}{T}\right)\tilde{v}_{\boldsymbol{k},\alpha}\partial_\alpha n + \\ &\times\frac{2\pi}{T}\left(h_\theta(z)+\tilde{h}_\theta(z)\frac{\theta_{\boldsymbol{k}}}{T}\right)\tilde{v}_{\boldsymbol{k},\alpha}\partial_\alpha\theta \\ &+\left(\delta_{\alpha\beta}\frac{\theta_{\boldsymbol{k}}}{T}-\frac{m v_{\boldsymbol{k},\alpha}v_{\boldsymbol{k},\beta}}{T}\right)\partial_\alpha u_\beta\Bigg]\bar{n}_{\boldsymbol{k}}(\bar{n}_{\boldsymbol{k}}+1). \qquad \text{(C6)}\end{aligned}$$

Using $n_{\boldsymbol{k}} = \bar{n}_{\boldsymbol{k}} + \delta n_{\boldsymbol{k}}$ and integrating over $\boldsymbol{k}$ leads to

$$\begin{aligned}P_{\alpha\beta} &= \frac{n\theta}{m}\delta_{\alpha\beta} + \nu(\partial_\alpha u_\beta + \partial_\beta u_\alpha) - \nu\delta_{\alpha\beta}\partial_\gamma u_\gamma, \\ q_\alpha &= \kappa_n\partial_\alpha n + \kappa_\theta\partial_\alpha\theta, \qquad \text{(C7)}\end{aligned}$$

where only linear terms on $\partial_\alpha n$, $\partial_\alpha\theta$, and $\partial_\alpha u_\beta$ were considered (i.e., gradients of thermodynamic quantities are small). For a 2D magnon gas with quadratic dispersion and collision rate of the form $1/\tau_{\boldsymbol{k}} \propto \boldsymbol{k}^2$ (i.e., only considering exchange coupling), the relaxation time yields that dissipation is dominated by viscosity $\nu(T,z) \sim \frac{J^2}{T}$, while $\kappa_n = \kappa_\theta$ are second-order effects (in powers of T/J) compared with ν; κ_n and κ_θ are dominated by deviations to quadratic dispersion and/or finite scattering at low scattering, e.g., dipolar interactions.

APPENDIX D: MEASUREMENT OF MAGNON SOUND MODES

We consider a spin-1/2 qubit with an intrinsic level splitting ω placed a distance d above the magnetic insulator. The dynamics of the qubit and the ferromagnet are governed by the Hamiltonian $\hat{H}_{\text{total}} = \hat{H} + \hat{H}_{\text{c}} + \hat{H}_{\text{q}}$. Here H_{F} is the Hamiltonian of the ferromagnet; see the main text. The term $\hat{H}_{\text{q}}$ is the qubit Hamiltonian given by $\hat{H}_{\text{q}} = \frac{1}{2}\omega\boldsymbol{n}_{\text{q}}\cdot\boldsymbol{\sigma}$, where $\boldsymbol{n}_{\text{q}}$ is the intrinsic polarizing field of the spin probe. For instance, in the case of NV centers in diamond, $\boldsymbol{n}_{\text{q}}$ is the axis of the NV defect in the diamond lattice. Finally, the term $\hat{H}_{\text{c}}$ is the qubit-ferromagnet coupling given by

$$H_{\text{c}} = \frac{\mu_{\text{B}}^2}{2}\hat{\boldsymbol{\sigma}}\cdot\hat{\boldsymbol{B}}, \quad \hat{\boldsymbol{B}} = \frac{1}{4\pi}\sum_j\left[\frac{\hat{\boldsymbol{S}}_j}{r_j^3} - \frac{3(\hat{\boldsymbol{S}}_j\cdot\boldsymbol{r}_j)\boldsymbol{r}_j}{r_j^5}\right], \qquad \text{(D1)}$$

where $\boldsymbol{B}$ is the magnetic field at the position of the probe induced by dipolar interactions with the 2D ferromagnet, and $\boldsymbol{r}_j = (x_j, y_j, -d)$ is the relative position between the i-th spin in the 2D lattice and probe.

In thermal equilibrium, the 2D ferromagnet is described by the density-matrix $\rho_{\text{F}} = \sum_n e^{-\varepsilon_n/k_{\text{B}}T}|n\rangle\langle n|$, where $|n\rangle$ are the eigenstates of the ferromagnet. The absorption rate, $1/T_{1,\text{abs}}$, and emission rate, $1/T_{1,\text{em}}$, is obtained from Fermi Golden's rule using the initial state $|i\rangle = |-\rangle\otimes\rho_{\text{F}}$ and $|i\rangle = |+\rangle\otimes\rho_{\text{F}}$, respectively,

$$1/T_{\text{abs,em}} = 2\pi\sum_{nm}\rho_n B^{\pm}_{nm}B^{\mp}_{mn}\delta(\omega\pm\varepsilon_{mn}). \qquad \text{(D2)}$$

Here B^α_{nm} denotes $\langle n|\hat{B}^\alpha|m\rangle$, and ε_{mn} is the energy difference between states m and n, $\varepsilon_{mn} = \varepsilon_m - \varepsilon_n$. The relaxation rate is defined as $1/T_1 = \frac{1}{2}[1/T_{\text{abs}} + T_{\text{em}}]$. More compactly, $1/T_1$ can be expressed as

$$\frac{1}{T_1} = \frac{\mu_{\text{B}}^2}{2}\int_{-\infty}^{\infty}dt e^{i\omega t}\langle\{\hat{B}^-(t),\hat{B}^+(0)\}\rangle. \qquad \text{(D3)}$$

For computation it is more convenient to express $1/T_1$ in terms of retarded correlation functions. In this direction, the fluctuation-dissipation theorem reads

$$\int_{-\infty}^{\infty}dt e^{i\omega t}\langle\{\hat{B}^-(t),\hat{B}^+(0)\}\rangle = \coth\left(\frac{\omega}{2T}\right)\text{Im}\left[\chi^{\text{R}}_{B^-B^+}(\omega)\right], \qquad \text{(D4)}$$

where $\chi^{\text{R}}_{B^-B^+}(\omega) = -i\int_0^\infty dt\langle[\hat{B}^-(t),\hat{B}^+(0)]\rangle$ is the retarded correlation function.

Finally, $1/T_1$ can be expressed in terms of spin-spin correlation functions. Expressing $\hat{S}^\alpha_\tau = \sum_{\boldsymbol{k}}\frac{e^{i\boldsymbol{k}\cdot\boldsymbol{\tau}}}{\sqrt{N}}\hat{S}^\alpha_{\boldsymbol{k}}$ in momentum space and inserting into Eq. (D1), we can express $\hat{B}^\alpha$ in terms of $S^\pm_{\boldsymbol{k}}$ and $S^z_{\boldsymbol{k}}$. Without loss of generality, we assume $\boldsymbol{k} = (k, 0)$. For $\hat{B}^x$, we find

$$\hat{B}^x_{\boldsymbol{k}} = \sum_j e^{ikx_j}\left[\left(\frac{1}{r_j^3}-\frac{3x_j^2}{r_j^5}\right)S^x_{\boldsymbol{k}} - \frac{3x_jy_j}{r_j^5}S^y_{\boldsymbol{k}} + \frac{3x_jd}{r_j^5}S^z_{\boldsymbol{k}}\right]. \qquad \text{(D5)}$$

Using the continuum approximation to approximate $\sum_j \to \frac{1}{a^2}\int d^2\boldsymbol{x}$, the first term on the right-hand side of Eq. (D5) is

$$\begin{aligned}\sum_j e^{ikx_j}\left(\frac{1}{r_j^3}-\frac{3x_j^2}{r_j^5}\right) &\to \frac{1}{a^2}\iint dxdy\, e^{ikx}\left(\frac{1}{r^3}-\frac{3x^2}{r^5}\right) \\ &= \frac{2}{a^2}\int dx e^{ikx}\frac{d^2-x^2}{(d^2+x^2)^2} \\ &= \frac{2}{da^2}\int d\xi e^{i(kd)\xi}\frac{1-\xi^2}{(1+\xi^2)^2}. \qquad \text{(D6)}\end{aligned}$$

In the last step, we can use the residue theorem to express $\int_{-\infty}^{\infty}d\xi e^{i(kd)\xi}\frac{1-\xi^2}{(1+\xi^2)^2}$ as $\oint dz e^{i(kd)z}\frac{1-z^2}{(1+z^2)^2} = \pi(kd)e^{-kd}$, where for $kd > 0$ we use a contour of integration in the upper-half complex plane. As a result, we obtain

$$\sum_j e^{ikx_j}\left(\frac{1}{r_j^3}-\frac{3x_j^2}{r_j^5}\right) \approx \frac{ke^{-kd}}{2a^2}, \qquad \text{(D7)}$$

exact in the continuum limit. For the second term on the right-hand side of Eq. (D5), we find $\sum_j e^{ikx_j}\frac{x_jy_j}{r_j^5} = 0$. Finally, for the third term in the right-hand side of Eq. (D5), we find

$$3\sum_j e^{ikx_j}\frac{x_jd}{r_j^5} \approx \frac{3ikd}{a^2}\iint dx\,dy\frac{x^2}{r^5} = \frac{ik}{2a^2}. \qquad \text{(D8)}$$

Repeating the same procedure for $\hat{B}^y$ and $\hat{B}^z$ and generalizing our results for a generic $\boldsymbol{k} = (k_x, k_y)$, we obtain $\hat{B}^\alpha = \frac{1}{\sqrt{N}}\sum_{\boldsymbol{k}}B^\alpha_{\boldsymbol{k}}$ with

$$\begin{pmatrix}\hat{B}^x_{\boldsymbol{k}}\\ \hat{B}^y_{\boldsymbol{k}}\\ \hat{B}^z_{\boldsymbol{k}}\end{pmatrix} = \frac{e^{-|\boldsymbol{k}|z}}{2a^2}\begin{pmatrix}k_x^2/|\boldsymbol{k}| & k_xk_y/|\boldsymbol{k}| & ik_x\\ k_xk_y/|\boldsymbol{k}| & k_y^2/|\boldsymbol{k}| & ik_y\\ ik_x & ik_y & -|\boldsymbol{k}|\end{pmatrix}\begin{pmatrix}\hat{S}^x_{\boldsymbol{k}}\\ \hat{S}^y_{\boldsymbol{k}}\\ \hat{S}^z_{\boldsymbol{k}}\end{pmatrix}. \qquad \text{(D9)}$$

The $B_{\boldsymbol{k}}^{\pm} = B_{\boldsymbol{k}}^{x} \pm iB_{\boldsymbol{k}}^{y}$ terms can be written as a function of $S_{\boldsymbol{k}}^{\pm}$ and $S_{\boldsymbol{k}}^{z}$ such that Eq. (D9) can be recasted as

$$\begin{pmatrix} \hat{B}_{\boldsymbol{k}}^{+} \\ \hat{B}_{\boldsymbol{k}}^{-} \\ \hat{B}_{\boldsymbol{k}}^{z} \end{pmatrix} = \frac{e^{-|\boldsymbol{k}|z}}{2a^2} \begin{pmatrix} |\boldsymbol{k}|/2 & (k_x + ik_y)^2/2|\boldsymbol{k}| & ik_x - k_y \\ (k_x - ik_y)^2/2|\boldsymbol{k}| & |\boldsymbol{k}|/2 & ik_x + k_y \\ (ik_x + k_y)/2 & (ik_x - k_y)/2 & -|\boldsymbol{k}| \end{pmatrix} \begin{pmatrix} \hat{S}_{\boldsymbol{k}}^{+} \\ \hat{S}_{\boldsymbol{k}}^{-} \\ \hat{S}_{\boldsymbol{k}}^{z} \end{pmatrix}. \tag{D10}$$

Using Eq. (D10) in Eq. (D3), the spin qubit relaxation time is given by

$$\frac{1}{T_1} = \coth\left(\frac{\omega}{2T}\right) \frac{\mu_{\mathrm{B}}^2}{2a^2} \int \frac{d^2\boldsymbol{k}}{(2\pi)^2} e^{-2|\boldsymbol{k}|d} |\boldsymbol{k}|^2 [\chi_{-+}^{\mathrm{R}}(\boldsymbol{k}, \omega) + \chi_{+-}^{\mathrm{R}}(\boldsymbol{k}, \omega) + 4\chi_{zz}^{\mathrm{R}}(\boldsymbol{k}, \omega)], \tag{D11}$$

where we denote $\chi_{\alpha\beta}^{\mathrm{R}}(\boldsymbol{k}, \omega) = -i \int_0^{\infty} dt \langle [\hat{S}_{-\boldsymbol{k}}^{\alpha}(t), \hat{S}_{\boldsymbol{k}}^{\beta}(0)] \rangle$.

APPENDIX E: TRANSVERSE SPIN FLUCTUATIONS

The spectral weight of the correlator $\chi_{+-}(\boldsymbol{k}, \omega) = -i \int_0^{\infty} dt e^{i\omega t} \langle [\hat{S}_{-\boldsymbol{k}}^{-}, S_{\boldsymbol{k}}^{+}(0)] \rangle$ is concentrated at the magnon frequency $\omega_{\boldsymbol{k}} = \Delta + \varepsilon_{\boldsymbol{k}}$ and is associated to the production of a single magnon. Off-resonant processes, however, give rise to a finite contribution to $\chi_{-+}(\boldsymbol{k}, \omega)$ below the magnon gap; see Fig. 4(a). As such, we estimate the contribution of such processes in the noise spectrum and show that they give a small contribution to χ_{+-} compared with that of the sound mode. With this objective in mind, we calculate the leading-order contribution of the imaginary part of the magnon self-energy $\Sigma(\boldsymbol{k}, \omega)$ and approximate the correlation function as

$$\chi_{+-}(\boldsymbol{k}, \omega) = \frac{1}{\omega - \omega_{\boldsymbol{k}} + i\Sigma''(\boldsymbol{k}, \omega)}, \tag{E1}$$

where energy shifts to the single magnon dispersion are neglected. From the effective interaction in Eq. (5) of the main text, this is given by the second-order process depicted in Fig. 4(b). In terms of Matsubara frequencies, it can be written as

$$\Sigma(\boldsymbol{k}, \omega) = -J^2 a^4 \sum_{\boldsymbol{pq}} \sum_{i\omega_n' i\omega_n''} (\boldsymbol{k} \cdot \boldsymbol{p})^2 \times \frac{1}{(i\omega_n' - \omega_{\boldsymbol{p}})(i\omega_n + i\omega_n'' - \omega_{\boldsymbol{k}+\boldsymbol{q}})(i\omega_n' - i\omega_n'' - \omega_{\boldsymbol{p}-\boldsymbol{q}})}. \tag{E2}$$

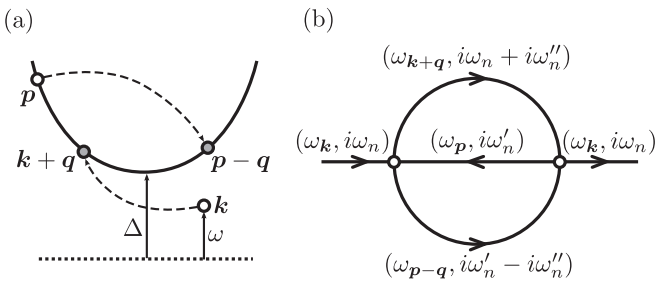

FIG. 4. (a) In addition to the sound mode, off-resonant processes can also give a finite contribution to χ_{-+} below the magnon gap. (b) Sunrise diagram contributing to the magnon self-energy of χ_{-+}.

The retarded correlator is obtained by analytical continuation $i\omega_n \to \omega + i\epsilon$ and taking the imaginary part of the resulting expression:

$$\Sigma''(\boldsymbol{k}, \omega) = J^2 a^4 \sum_{\boldsymbol{pq}} (\boldsymbol{k} \cdot \boldsymbol{p})^2 \delta(\omega - \Delta + \varepsilon_{\boldsymbol{p}} - \varepsilon_{\boldsymbol{k}+\boldsymbol{q}} - \varepsilon_{\boldsymbol{p}-\boldsymbol{q}})(n_{\boldsymbol{p}} - \tilde{n}_{\boldsymbol{p}})(1 + n_{\boldsymbol{k}+\boldsymbol{q}} + n_{\boldsymbol{p}-\boldsymbol{q}}), \tag{E3}$$

where we denote $\tilde{n}_{\boldsymbol{p}} = n(\varepsilon_{\boldsymbol{p}} + \omega)$. A similar analysis follows for the correlator $\chi_{+-}(\omega) \approx \delta(\omega + \omega_{\boldsymbol{k}})$. Dimensional analysis in the limit $\omega \ll T$ yields Σ'' scaling as $\Sigma(\boldsymbol{q}, \omega) = \frac{T\omega}{J}(qa)^2$.

APPENDIX F: EFFECT OF DIPOLAR INTERACTIONS

Dipolar interactions, which can be sizable in a 2D ferromagnet, introduce a variety of effects that need to be carefully taken into account, namely, it modifies the collision term by adding hard-core repulsion and induces magnon leakage via three-body interactions. We incorporate dipolar interactions via the term

$$\hat{H}_{\mathrm{d}} = \frac{\mu_{\mathrm{B}}^2}{4\pi} \frac{1}{2} \sum_{jj'} \left[\frac{\hat{\boldsymbol{S}}_j \cdot \hat{\boldsymbol{S}}_{j'}}{r_{jj'}^3} - 3 \frac{(\hat{\boldsymbol{S}}_j \cdot \boldsymbol{r}_{jj'})(\hat{\boldsymbol{S}}_{j'} \cdot \boldsymbol{r}_{jj'})}{r_{jj'}^5} \right], \tag{F1}$$

where μ_{B} is the Bohr magneton, and $\boldsymbol{r}_{jj'}$ is the relative distance between spins j and j'. It is important to consider the combined effect of the Zeeman term,

$$\hat{H}_{\mathrm{z}} = \Delta \sum_i \hat{S}_i^z, \tag{F2}$$

and dipolar interactions. In particular, in the presence of a Zeeman field, it is convenient to pick a quantization axis which is canted from the 2D plane $\boldsymbol{r} = (x, y, 0)$,

$$\begin{aligned} \hat{S}_j^z &\to \cos\theta \hat{S}_j^z - \sin\theta \hat{S}_j^x, \\ \hat{S}_j^x &\to \cos\theta \hat{S}_j^x + \sin\theta \hat{S}_j^z, \\ \hat{S}_j^y &\to \hat{S}_j^y, \end{aligned} \tag{F3}$$

where θ will be conveniently chosen below. Inserting Eq. (F3) into Eq. (F1), we find

$$\hat{H}_{\rm d} = \frac{\mu_{\rm B}^2}{8\pi}\sum_{j\tau}\frac{1}{\tau^3}\Bigg[\hat{S}_j^x\hat{S}_{j+\tau}^x\left(1-3\cos^2\theta\frac{\tau_x^2}{\tau^2}\right)+\hat{S}_j^y\hat{S}_{j+\tau}^y\left(1-3\frac{\tau_y^2}{\tau^2}\right)+\hat{S}_j^z\hat{S}_{j+\tau}^z\left(1-3\sin^2\theta\frac{\tau_x^2}{\tau^2}\right)$$
$$-6\sin\theta\cos\theta\frac{\tau_x^2}{\tau^2}\hat{S}_j^x\hat{S}_{j+\tau}^z-6\cos\theta\frac{\tau_x\tau_y}{\tau^2}\hat{S}_j^x\hat{S}_{j+\tau}^y-6\sin\theta\frac{\tau_x\tau_y}{\tau^2}\hat{S}_j^z\hat{S}_{j+\tau}^y\Bigg], \tag{F4}$$

where τ denotes relative positions between spins on a 2D square lattice (not restricted to nearest neighbors). After rearranging terms, we find

$$\hat{H}_{\rm d} = \frac{3\mu_{\rm B}^2}{8\pi}\sum_{j\tau}\frac{1}{\tau^3}\Bigg[(\hat{\mathbf{S}}_j\cdot\hat{\mathbf{S}}_{j+\tau})\left(\frac{1}{3}-\frac{\tau_x^2}{\tau^2}\right)+\sin^2\theta\frac{\tau_x^2}{\tau^2}\hat{S}_j^x\hat{S}_{j+\tau}^x+\cos^2\theta\frac{\tau_x^2}{\tau^2}\hat{S}_j^z\hat{S}_{j+\tau}^z-\frac{\tau_y^2-\tau_x^2}{\tau^5}\hat{S}_j^y\hat{S}_{j+\tau}^y$$
$$-2\sin\theta\cos\theta\frac{\tau_x^2}{\tau^2}\hat{S}_j^x\hat{S}_{j+\tau}^z-2\cos\theta\frac{\tau_x\tau_y}{\tau^2}\hat{S}_j^x\hat{S}_{j+\tau}^y-2\sin\theta\frac{\tau_x\tau_y}{\tau^2}\hat{S}_j^z\hat{S}_{j+\tau}^y\Bigg]. \tag{F5}$$

Note that the first term on the right-hand side can be incorporated into the definition of J with a small anisotropy in the x direction which we will neglect. For convenience, we define $\hat{H}_{\rm d} = \hat{H}_{zz}+\hat{H}_{xz}+\hat{H}_{xx}+\hat{H}_{yy}+\hat{H}_{xy}+\hat{H}_{yz}$, with

$$\hat{H}_{zz} = \varepsilon_{\rm d}\cos^2\theta\frac{a^3}{\pi S^2}\sum_{j\tau}\frac{\tau_x^2}{\tau^5}\hat{S}_j^z\hat{S}_{j+\tau}^z,\ \hat{H}_{xx} = \varepsilon_{\rm d}\sin^2\theta\frac{a^3}{\pi S^2}\sum_{j\tau}\frac{\tau_x^2}{\tau^5}\hat{S}_j^x\hat{S}_{j+\tau}^x,\ \hat{H}_{xz} = -2\varepsilon_{\rm d}\sin\theta\cos\theta\frac{a^3}{\pi S^2}\sum_{j\tau}\frac{\tau_x\tau_y}{\tau^5}\hat{S}_j^x\hat{S}_{j+\tau}^z,$$
$$\hat{H}_{yy} = \varepsilon_{\rm d}\frac{a^3}{\pi S^2}\sum_{j\tau}\frac{\tau_y^2-\tau_x^2}{\tau^5}\hat{S}_j^y\hat{S}_{j+\tau}^y,\ \hat{H}_{xy} = -2\varepsilon_{\rm d}\cos\theta\frac{a^3}{\pi S^2}\sum_{j\tau}\frac{\tau_x\tau_y}{\tau^5}\hat{S}_j^x\hat{S}_{j+\tau}^y,\quad \hat{H}_{yz} = -2\varepsilon_{\rm d}\sin\theta\frac{a^3}{\pi S^2}\sum_{j\tau}\frac{\tau_x\tau_y}{\tau^5}\hat{S}_j^y\hat{S}_{j+\tau}^z, \tag{F6}$$

where we defined the dipolar energy as

$$\varepsilon_{\rm d} = \frac{3S^2\mu_{\rm B}^2}{4a^3}. \tag{F7}$$

The Zeeman splitting term in the rotated frame is given $\hat{H}_{\rm z} = \hat{H}_x+\hat{H}_z$, with

$$\hat{H}_x = \Delta\cos\theta\sum_j\hat{S}_j^x,\quad \hat{H}_z = -\Delta\sin\theta\sum_j\hat{S}_j^z. \tag{F8}$$

Focusing on $\hat{H}_{zz}$ first, we define $\hat{S}_j^z = -S(1-\hat{n}_j)$, which leads to

$$\hat{H}_{zz} = \varepsilon_{\rm d}\cos^2\theta\frac{a^3}{\pi}\sum_{j\tau}\frac{\tau_x^2}{\tau^5}(1-2\hat{n}_j+\hat{n}_j\hat{n}_{j+\tau}) = \varepsilon_{\rm d}\cos^2\theta\left(NS-2\sum_j\hat{n}_j+\frac{a^3}{\pi}\sum_{j\tau}\frac{\tau_x^2}{\tau^5}\hat{n}_j\hat{n}_{j+\tau}\right), \tag{F9}$$

and where, in the last step, we used

$$\sum_{\boldsymbol{\tau}}e^{-i\mathbf{k}\cdot\boldsymbol{\tau}}\frac{\tau_x^2}{\tau^5} = \frac{\pi}{a^3}+O(q^2). \tag{F10}$$

Similarly, for $\hat{H}_{xz}$ we find

$$\hat{H}_{xz} = 2\varepsilon_{\rm d}\sin\theta\cos\theta\frac{a^3}{\pi S}\sum_{j\tau}\frac{\tau_x^2}{\tau^5}\hat{S}_j^x(1-\hat{n}_{j+\tau}) = \frac{2\varepsilon_{\rm d}\sin\theta\cos\theta}{S}\left(\sum_j\hat{S}_j^x-\frac{a^3}{\pi}\sum_{j\tau}\frac{\tau_x^2}{\tau^5}\hat{S}_j^x\hat{n}_{j+\tau}\right). \tag{F11}$$

Turning to $\hat{H}_{xx}$ and using $\hat{S}_j^x = (\hat{S}_j^+ + \hat{S}_j^-)/2$, we find

$$\hat{H}_{xx} = \frac{\varepsilon_{\rm d}\sin^2\theta}{4}\frac{a^3}{\pi S^2}\sum_{j\tau}\frac{\tau_x^2}{\tau^5}(\hat{S}_j^+\hat{S}_{j+\tau}^+ + \hat{S}_j^-\hat{S}_{j+\tau}^- + 2\hat{S}_j^+\hat{S}_{j+\tau}^-) = \frac{\varepsilon_{\rm d}\sin^2\theta}{4S^2}\sum_{\boldsymbol{k}}(\hat{S}_{-\boldsymbol{k}}^+\hat{S}_{\boldsymbol{k}}^+ + \hat{S}_{-\boldsymbol{k}}^-\hat{S}_{\boldsymbol{k}}^- + 2\hat{S}_{-\boldsymbol{k}}^+\hat{S}_{\boldsymbol{k}}^-), \tag{F12}$$

where, in the last step, we used Eq. (F10). The term $\hat{H}_{xx}$ introduces coherent creation/destruction of two magnons. The term $\hat{H}_{xy}$ also introduces similar two-magnon processes such as those in $\hat{H}_{xx}$,

$$\hat{H}_{xy} = -\frac{\varepsilon_{\rm d}\cos\theta}{2i}\frac{a^3}{\pi S^2}\sum_{j\tau}\frac{\tau_x\tau_y}{|\boldsymbol{\tau}|^5}(\hat{S}_j^+\hat{S}_{j+\tau}^+ - \hat{S}_j^-\hat{S}_{j+\tau}^-) = -\frac{2\varepsilon_{\rm d}\cos\theta}{i\pi S^2}\sum_{\boldsymbol{k}}\frac{k_xk_y}{a}(\hat{S}_{-\boldsymbol{k}}^+\hat{S}_{\boldsymbol{k}}^+ - \hat{S}_{-\boldsymbol{k}}^-\hat{S}_{\boldsymbol{k}}^-), \tag{F13}$$

but the matrix elements of $\hat{H}_{xy}$ are $O(q^2)$ smaller than those corresponding to $\hat{H}_{xx}$ [in the last step of Eq. (F13), we used $\sum_{\boldsymbol{\tau}} e^{i\boldsymbol{k}\cdot\boldsymbol{\tau}} \frac{\tau_x\tau_y}{\tau^5} = \frac{4k_xk_y}{a} + O(k^4)$]. As a result, we neglect $\hat{H}_{xy}$. Finally, for $\hat{H}_{yz}$, we find

$$\begin{aligned}\hat{H}_{yz} = & \quad -2\varepsilon_{\rm d}\sin\theta\tfrac{a^3}{\pi S}\textstyle\sum_{j\tau}\frac{\tau_x\tau_y}{\tau^5}\hat{S}^y_j(1-n_{j+\tau}) = -2\varepsilon_{\rm d}\sin\theta\tfrac{a^3}{\pi S}\big(\textstyle\sum_{j\tau}\frac{\tau_x\tau_y}{\tau^5}\hat{S}^y_j - \sum_{j\tau}\frac{\tau_x\tau_y}{\tau^5}\hat{S}^y_j\hat{n}_{j+\tau}\big)\\ = & \quad 6\varepsilon_{\rm d}\sin\theta\tfrac{a^3}{\pi S}\textstyle\sum_{j\tau}\frac{\tau_x\tau_y}{\tau^5}\hat{S}^y_j\hat{n}_{j+\tau},\end{aligned} \tag{F14}$$

where the first term in the third equality is zero because $\sum_{\boldsymbol{\tau}} \tau_x\tau_y/\tau^5 = 0$, thus giving only a cubic term. The cubic term, however, has matrix elements $O(q^2)$ smaller than those corresponding to $\hat{H}_{xz}$ because of the factors $\tau_x\tau_y$. As a result, we neglect the matrix elements introduced by $\hat{H}_{yz}$ when compared with those in $\hat{H}_{xz}$.

The Zeeman splitting term $\hat{H}_x$ and the dipolar term $\hat{H}_{xz}$ both generate terms which are linear in $\hat{S}^x_i$. In particular,

$$\hat{H}_x + \hat{H}_{xz} = -\Delta\sin\theta\sum_j \hat{S}^x_j + \frac{2\varepsilon_{\rm d}\sin\theta\cos\theta}{S}\sum_j \hat{S}^x_j - \frac{2\varepsilon_{\rm d}\sin\theta\cos\theta}{S}\sum_{j\tau}\frac{\tau_x^2}{\tau^5}\hat{S}^x_j\hat{n}_{j+\tau}. \tag{F15}$$

As a result, we conveniently define θ such that the linear term is canceled. This leads to

$$\begin{aligned}\cos\theta &= \frac{S\Delta}{2\varepsilon_{\rm d}}, \quad 0 \leqslant S\Delta \leqslant 2\varepsilon_{\rm d},\\ \theta &= 0, \quad S\Delta > 2\varepsilon_{\rm d}.\end{aligned} \tag{F16}$$

Therefore in this case, the terms

$$\hat{H}_x + \hat{H}_{xz} = -\frac{2\varepsilon_{\rm d}\sin\theta\cos\theta}{S}\sum_{j\tau}\frac{\tau_x^2}{\tau^5}\hat{S}^x_j\hat{n}_{j+\tau} \tag{F17}$$

lead to a cubic interaction term after a Holstein-Primakoff transformation.

In the same spirit, combining $\hat{H}_z$ from Zeeman splitting and $\hat{H}_{zz}$ from dipolar interaction, we find

$$\hat{H}_z + \hat{H}_{zz} = (\Delta S\cos\theta - 2\varepsilon_{\rm d}\cos^2\theta)\sum_j \hat{n}_j + \varepsilon_{\rm d}\cos^2\theta\frac{a^3}{\pi}\sum_{j\tau}\frac{\tau_x^2}{\tau^5}\hat{n}_j\hat{n}_{j+\tau}. \tag{F18}$$

As a result, the combination of H_z and H_{zz} gives rise to a magnon gap induced by Zeeman splitting and dipolar interactions and a quartic interaction induced by dipolar interactions.

1. Effective Hamiltonian

To cast the dipolar Hamiltonian into a long-wavelength, effective Hamiltonian, we use the Holstein-Primakoff transformation to leading order, which results in

$$\sum_{j\tau}\frac{\tau_x^2}{\tau^5}\hat{n}_j\hat{n}_{j+\tau} = \sum_{j\tau}\frac{\tau_x^2}{\tau^5}\hat{a}^\dagger_j\hat{a}^\dagger_{j+\tau}\hat{a}_{j+\tau}\hat{a}_j = \sum_{\boldsymbol{kpq}}\left(\sum_\tau e^{-i\boldsymbol{q}\cdot\boldsymbol{\tau}}\frac{\tau_x^2}{\tau^5}\right)\hat{a}^\dagger_{\boldsymbol{k}+\boldsymbol{q}}\hat{a}^\dagger_{\boldsymbol{p}-\boldsymbol{q}}\hat{a}_{\boldsymbol{p}}\hat{a}_{\boldsymbol{k}} \approx \frac{\pi}{a^3}\sum_{\boldsymbol{kpq}}\hat{a}^\dagger_{\boldsymbol{k}+\boldsymbol{q}}\hat{a}^\dagger_{\boldsymbol{p}-\boldsymbol{q}}\hat{a}_{\boldsymbol{p}}\hat{a}_{\boldsymbol{k}}. \tag{F19}$$

In the last step, we used Eq. (F10). In addition, for Eq. (F17) we use

$$\begin{aligned}\sum_{j\tau}\frac{\tau_x^2}{\tau^5}\hat{S}^x_j\hat{n}_{j+\tau} &= \sqrt{\frac{S}{2}}\sum_{j\tau}\frac{\tau_x^2}{\tau^5}(\hat{a}^\dagger_j\hat{a}^\dagger_{j+\tau}\hat{a}_{j+\tau} + \hat{a}^\dagger_{j+\tau}\hat{a}_{j+\tau}\hat{a}_j) = \sqrt{\frac{S}{2N}}\sum_{\boldsymbol{kp\tau}}\frac{\tau_x^2}{\tau^5}[e^{-\boldsymbol{p}\cdot\boldsymbol{\tau}}\hat{a}^\dagger_{\boldsymbol{p}}\hat{a}^\dagger_{\boldsymbol{k}}\hat{a}_{\boldsymbol{k}+\boldsymbol{p}} + e^{-i\boldsymbol{k}\cdot\boldsymbol{p}}\hat{a}^\dagger_{\boldsymbol{k}+\boldsymbol{p}}\hat{a}_{\boldsymbol{p}}\hat{a}_{\boldsymbol{k}}]\\ &\approx \sqrt{\frac{S}{2N}}\frac{\pi}{a^3}\sum_{\boldsymbol{kp}}(\hat{a}^\dagger_{\boldsymbol{p}}\hat{a}^\dagger_{\boldsymbol{k}}\hat{a}_{\boldsymbol{k}+\boldsymbol{p}} + \hat{a}^\dagger_{\boldsymbol{k}+\boldsymbol{p}}\hat{a}_{\boldsymbol{p}}\hat{a}_{\boldsymbol{k}}).\end{aligned} \tag{F20}$$

Putting everything together, we find that, at long wavelength, the dipolar and Zeeman Hamiltonian can be effectively written as

$$\begin{aligned}&\hat{H}_{\rm d} + \hat{H}_z \approx \sum_{\boldsymbol{k}}[\Delta\hat{a}^\dagger_{\boldsymbol{k}}\hat{a}_{\boldsymbol{k}} + \lambda_2(\hat{a}_{\boldsymbol{k}}\hat{a}_{-\boldsymbol{k}} + \hat{a}^\dagger_{\boldsymbol{k}}\hat{a}^\dagger_{-\boldsymbol{k}})] - \frac{\lambda_3}{\sqrt{N}}\sum_{\boldsymbol{kp}}(\hat{a}^\dagger_{\boldsymbol{p}}\hat{a}^\dagger_{\boldsymbol{k}}\hat{a}_{\boldsymbol{k}+\boldsymbol{p}} + \hat{a}^\dagger_{\boldsymbol{k}+\boldsymbol{p}}\hat{a}_{\boldsymbol{p}}\hat{a}_{\boldsymbol{k}}) + \frac{\lambda_4}{N}\sum_{\boldsymbol{kpq}}a^\dagger_{\boldsymbol{p}+\boldsymbol{q}}\hat{a}^\dagger_{\boldsymbol{k}-\boldsymbol{q}}\hat{a}_{\boldsymbol{p}}\hat{a}_{\boldsymbol{k}},\\ &\tilde{\Delta} = (\Delta S\cos\theta - 2\varepsilon_{\rm d}\cos^2\theta) + \frac{\varepsilon_{\rm d}\sin^2\theta}{S}, \quad \lambda_2 = \frac{\varepsilon_{\rm d}\sin^2\theta}{2S}, \quad \lambda_3 = \varepsilon_{\rm d}\sqrt{2/S}\sin\theta\cos\theta, \quad \lambda_4 = \varepsilon_{\rm d}\cos^2\theta.\end{aligned} \tag{F21}$$

2. Bogoliubov transformation

For small Zeeman fields, the canting angle lies in the range $0 < \theta \leqslant \pi/2$, and $\lambda_{2,3}$ are finite. The quadratic part of the Heisenberg Hamiltonian combined with Eq. (F21),

$$\hat{H}_2 = \sum_{\boldsymbol{k}} [(\Delta + \varepsilon_{\boldsymbol{k}})\hat{a}^\dagger_{\boldsymbol{k}}\hat{a}_{\boldsymbol{k}} + \lambda_2(\hat{a}_{\boldsymbol{k}}\hat{a}_{-\boldsymbol{k}} + \hat{a}^\dagger_{\boldsymbol{k}}\hat{a}^\dagger_{-\boldsymbol{k}})], \tag{F22}$$

can be diagonalized using a Bogoliubov transformation:

$$\hat{a}_{\boldsymbol{k}} = s_{\boldsymbol{k}}\hat{\beta}_{\boldsymbol{k}} + t_{\boldsymbol{k}}\hat{\gamma}^\dagger_{-\boldsymbol{k}}, \quad \hat{a}_{-\boldsymbol{k}} = s_{\boldsymbol{k}}\hat{\beta}_{\boldsymbol{k}} + t_{\boldsymbol{k}}\hat{\gamma}^\dagger_{-\boldsymbol{k}}, \tag{F23}$$

where $s_{\boldsymbol{k}}$ and $t_{\boldsymbol{k}}$ are $\boldsymbol{k}$-dependent real numbers. It is straightforward to show that

$$s_{\boldsymbol{k}} = \cosh\varphi_{\boldsymbol{k}}, \quad t_{\boldsymbol{k}} = \sinh\varphi_{\boldsymbol{k}}, \tag{F24}$$

diagonalizes $\hat{H}_2$,

$$\hat{H}_2 = \sum_{\boldsymbol{k}} E_{\boldsymbol{k}}[\beta^\dagger_{\boldsymbol{k}}\beta_{\boldsymbol{k}} + \gamma^\dagger_{\boldsymbol{k}}\gamma_{\boldsymbol{k}}], \quad E_{\boldsymbol{k}} = \sqrt{(\varepsilon_{\boldsymbol{k}} + \Delta)^2 - \lambda_2^2}, \tag{F25}$$

where $\varphi_{\boldsymbol{k}}$ is the solution of

$$\sinh 2\varphi_{\boldsymbol{k}} = -\frac{\lambda_2}{2E_{\boldsymbol{k}}}. \tag{F26}$$

Several comments are in order. First, we note that the magnon dispersion is quadratic, with or without dipolar interactions. In particular, in the presence of dipolar interactions, there will be a small correction to the magnon mass at low energies on the order of $\mathcal{O}(\varepsilon_{\rm d}/J)$, and which we will neglect (quadratic dispersion greatly simplifies the hydrodynamic description, as will be discussed below). Second, we are mainly interested in the hydrodynamic behavior at large T such that magnon–magnon collisions become important. In the regime $\varepsilon_{\rm d} \ll T \ll J$, most magnons will typically have large kinetic energies $\varepsilon_{\boldsymbol{k}}$ such that corrections due to the Bogoliubov transformation are negligible.

For sufficiently large Zeeman fields, when $\Delta \geqslant \varepsilon_{\rm d}$ and $\theta = 0$, then the coupling terms verify $\lambda_{2,3} = 0$. In this case, the quadratic part of $\hat{H}_J + \hat{H}_{\rm d} + \hat{H}_{\rm z}$ is already diagonal in the $(\hat{a}_{\boldsymbol{k}}, a^\dagger_{\boldsymbol{k}})$ basis and there is no need for a Bogoliubov transformation.

3. Magnon leakage

Three magnon processes in Eq.(F21) do not preserve particle number. This means that the distribution function $\bar{n}_{\boldsymbol{k}} = [z^{-1}e^{\varepsilon_{\boldsymbol{k}}/T} - 1]^{-1}$ is a quasiequilibrium distribution if $0 < z < 1$ and invalidates our hydrodynamic theory for frequencies below the leakage rate. The total magnon leakage rate can be calculated from

$$\frac{dn}{dt} = -\frac{\lambda_3^2}{N^2}\sum_{\boldsymbol{kp}} 2\pi\,\delta(\varepsilon_{\boldsymbol{k}} + \varepsilon_{\boldsymbol{p}} + \Delta - \varepsilon_{\boldsymbol{k}+\boldsymbol{p}}) \times [\bar{n}_{\boldsymbol{k}}\bar{n}_{\boldsymbol{p}}(1 + \bar{n}_{\boldsymbol{k}+\boldsymbol{p}}) - (1 + \bar{n}_{\boldsymbol{k}})(1 + \bar{n}_{\boldsymbol{p}})\bar{n}_{\boldsymbol{k}+\boldsymbol{p}}]. \tag{F27}$$

Here we note that three magnon processes are not necessarily suppressed by energy and momenta conservation. For instance, if the incoming magnon states have momenta that verify $\boldsymbol{k}\cdot\boldsymbol{p} = m\Delta$, then energy and momentum are conserved after the collision. For concreteness, let us assume that $u_\alpha \ll \sqrt{T/m}$, which leads to

$$\frac{dn}{dt} = -\frac{\gamma_{\rm leak}(z^2 - z^3)}{4\pi}\frac{T\lambda_3^2}{J^2a^2}, \tag{F28}$$

where we normalized $\tilde{\boldsymbol{k}} = \boldsymbol{k}/\bar{k}$ and the value of $\gamma_{\rm leak}(z)$ can be shown numerically to be $\gamma_{\rm leak} \sim \mathcal{O}(1)$. From here we can define the leakage rate

$$\frac{1}{\tau_{\rm leak}} = \frac{1}{n}\frac{dn}{dt} = \frac{\gamma_{\rm leak}\lambda_3^2}{2J}(z^2 - z^3). \tag{F29}$$

Using $J \sim 1000\,\mathrm{K}$, $\lambda_3 \sim 1\,\mathrm{K}$, and $z \approx 0.9$, we obtain $1/\tau_{\rm leak} \sim 5\,\mathrm{MHz}$. As such, the magnon number can be assumed to be a good conserved quantity for $\omega \gg 1\,\mathrm{MHz}$.

[1] I. Torre, A. Tomadin, A. K. Geim, and M. Polini, Phys. Rev. B **92**, 165433 (2015).
[2] D. A. Bandurin, I. Torre, R. K. Kumar, M. Ben Shalom, A. Tomadin, A. Principi, G. H. Auton, E. Khestanova, K. S. Novoselov, I. V. Grigorieva, L. A. Ponomarenko, A. K. Geim, and M. Polini, Science **351**, 1055 (2016).
[3] J. Crossno, J. K. Shi, K. Wang, X. Liu, A. Harzheim, A. Lucas, S. Sachdev, P. Kim, T. Taniguchi, K. Watanabe, T. A. Ohki, and K. C. Fong, Science **351**, 1058 (2016).
[4] L. Levitov and G. Falkovich, Nat. Phys. **12**, 672 (2016).
[5] H. Guo, E. Ilseven, G. Falkovich, and L. S. Levitov, Proc. Natl. Acad. Sci. **114**, 3068 (2017).
[6] R. Krishna Kumar, D. A. Bandurin, F. M. D. Pellegrino, Y. Cao, A. Principi, H. Guo, G. Auton, M. Ben Shalom, L. A. Ponomarenko, G. Falkovich, K. Watanabe, T. Taniguchi, I. Grigorieva, L. S. Levitov, M. Polini, and A. Geim, Nat. Phys. **13**, 1182 (2017).
[7] R. A. Davison, L. V. Delacrétaz, B. Goutéraux, and S. A. Hartnoll, Phys. Rev. B **94**, 054502 (2016).
[8] A. Lucas, Phys. Rev. B **93**, 245153 (2016).
[9] A. Lucas, R. A. Davison, and S. Sachdev, Proc. Natl. Acad. Sci. **113**, 9463 (2016).
[10] O. A. Castro-Alvaredo, B. Doyon, and T. Yoshimura, Phys. Rev. X **6**, 041065 (2016).
[11] V. B. Bulchandani, R. Vasseur, C. Karrasch, and J. E. Moore, Phys. Rev. Lett. **119**, 220604 (2017).
[12] A. Lucas and S. A. Hartnoll, Proc. Natl. Acad. Sci. **114**, 11344 (2017).
[13] V. Scopelliti, K. Schalm, and A. Lucas, Phys. Rev. B **96**, 075150 (2017).
[14] L. V. Delacrétaz, B. Goutéraux, S. A. Hartnoll, and A. Karlsson, Phys. Rev. B **96**, 195128 (2017).
[15] L. V. Delacrétaz and A. Gromov, Phys. Rev. Lett. **119**, 226602 (2017).
[16] T. Scaffidi, N. Nandi, B. Schmidt, A. P. Mackenzie, and J. E. Moore, Phys. Rev. Lett. **118**, 226601 (2017).
[17] L. Rondin, J.-P. Tetienne, T. Hingant, J.-F. Roch, P. Maletinsky, and V. Jacques, Rep. Prog. Phys. **77**, 056503 (2014).

[18] C. L. Degen, F. Reinhard, and P. Cappellaro, Rev. Mod. Phys. **89**, 035002 (2017).
[19] F. J. Dyson, Phys. Rev. **102**, 1217 (1956).
[20] G. F. Reiter, Phys. Rev. **175**, 631 (1968).
[21] K. Michel and F. Schwabl, Solid State Commun. **7**, 1781 (1969).
[22] K. H. Michel and F. Schwabl, Phys. Kondens. Mater. **11**, 144 (1970).
[23] A. Lucas and S. Das Sarma, Phys. Rev. B **97**, 115449 (2018).
[24] S. O. Demokritov, V. E. Demidov, O. Dzyapko, G. A. Melkov, A. A. Serga, B. Hillebrands, and A. N. Slavin, Nature (London) **443**, 430 (2006).
[25] V. E. Demidov, O. Dzyapko, S. O. Demokritov, G. A. Melkov, and A. N. Slavin, Phys. Rev. Lett. **99**, 037205 (2007).
[26] D. A. Bozhko, A. J. E. Kreil, H. Y. Musiienko-Shmarova, A. A. Serga, A. Pomyalov, V. S. Lvov, and B. Hillebrands, Nat. Commun. **10**, 2460 (2019).
[27] V. Tiberkevich, I. V. Borisenko, P. Nowik-Boltyk, V. E. Demidov, A. B. Rinkevich, S. O. Demokritov, and A. N. Slavin, Sci. Rep. **9**, 9063 (2019).
[28] E. Iacocca, T. J. Silva, and M. A. Hoefer, Phys. Rev. Lett. **118**, 017203 (2017).
[29] E. Demler and A. Maltsev, Ann. Phys. **326**, 1775 (2011), july 2011 Special Issue.
[30] E. A. Demler, A. Y. Maltsev, and A. O. Prokofiev, J. Phys. B: At. Mol. Opt. Phys. **50**, 124001 (2017).
[31] J. F. Rodriguez-Nieva, A. Schuckert, D. Sels, M. Knap, and E. Demler, Phys. Rev. B **105**, L060302 (2022).
[32] B. I. Halperin and P. C. Hohenberg, Phys. Rev. **188**, 898 (1969).
[33] After this work was posted online, an experiment in YIG came out suggesting measuring a second sound mode [27].
[34] T. van der Sar, F. Casola, R. Walsworth, and A. Yacoby, Nat. Commun. **6**, 7886 (2015).
[35] C. Du, T. van der Sar, T. X. Zhou, P. Upadhyaya, F. Casola, H. Zhang, M. C. Onbasli, C. A. Ross, R. L. Walsworth, Y. Tserkovnyak, and A. Yacoby, Science **357**, 195 (2017).
[36] S. Hild, T. Fukuhara, P. Schauß, J. Zeiher, M. Knap, E. Demler, I. Bloch, and C. Gross, Phys. Rev. Lett. **113**, 147205 (2014).
[37] R. C. Brown, R. Wyllie, S. B. Koller, E. A. Goldschmidt, M. Foss-Feig, and J. V. Porto, Science **348**, 540 (2015).
[38] A. B. Bardon, S. Beattie, C. Luciuk, W. Cairncross, D. Fine, N. S. Cheng, G. J. A. Edge, E. Taylor, S. Zhang, S. Trotzky, and J. H. Thywissen, Science **344**, 722 (2014).
[39] P. N. Jepsen, J. Amato-Grill, I. Dimitrova, W. W. Ho, E. Demler, and W. Ketterle, Nature (London) **588**, 403 (2020).
[40] M. S. Grinolds, S. Hong, P. Maletinsky, L. Luan, M. D. Lukin, R. L. Walsworth, and A. Yacoby, Nat. Phys. **9**, 215 (2013).
[41] J.-P. Tetienne, T. Hingant, L. Martínez, S. Rohart, A. Thiaville, L. H. Diez, K. Garcia, J.-P. Adam, J.-V. Kim, J.-F. Roch, I. Miron, G. Gaudin, L. Vila, B. Ocker, D. Ravelosona, and V. Jacques, Nat. Commun. **6**, 6733 (2015).
[42] S. Kolkowitz, A. Safira, A. A. High, R. C. Devlin, S. Choi, Q. P. Unterreithmeier, D. Patterson, A. S. Zibrov, V. E. Manucharyan, H. Park, and M. D. Lukin, Science **347**, 1129 (2015).
[43] K. Agarwal, R. Schmidt, B. Halperin, V. Oganesyan, G. Zaránd, M. D. Lukin, and E. Demler, Phys. Rev. B **95**, 155107 (2017).
[44] J. F. Rodriguez-Nieva, K. Agarwal, T. Giamarchi, B. I. Halperin, M. D. Lukin, and E. Demler, Phys. Rev. B **98**, 195433 (2018).
[45] B. Flebus and Y. Tserkovnyak, Phys. Rev. Lett. **121**, 187204 (2018).
[46] S. Chatterjee, J. F. Rodriguez-Nieva, and E. Demler, Phys. Rev. B **99**, 104425 (2019).
[47] In fact, not only is $|\boldsymbol{k},\boldsymbol{p}\rangle = S^+_{\boldsymbol{k}} S^+_{\boldsymbol{p}}|\mathrm{F}\rangle$ not diagonal, but they are not properly normalized nor do they form an orthogonal basis, see discussion in Supplement.
[48] D. C. Mattis, *The Theory of Magnetism Made Simple* (World Scientific, 2006), Sec. 5.3.
[49] B. Flebus, S. A. Bender, Y. Tserkovnyak, and R. A. Duine, Phys. Rev. Lett. **116**, 117201 (2016).
[50] A. J. Princep, R. A. Ewings, S. Ward, S. TÃ³th, C. Dubs, D. Prabhakaran, and A. T. Boothroyd, npj Quantum Mater. **2**, 63 (2017).